Title

Sulfate (re-)cycling in the oceanic crust: Effects of seawater-rock interaction, sulfur reduction and temperature on the abundance and isotope composition of anhydrite

Authors

Kleine, Barbara I
Stefánsson, Andri
Zierenberg, Robert A
et al.

Publication Date

2022

DOI

10.1016/j.gca.2021.10.016

Peer reviewed

Available online at www.sciencedirect.com

ScienceDirect

Geochimica et Cosmochimica Acta 317 (2022) 65–90

Geochimica et Cosmochimica Acta

www.elsevier.com/locate/gca

Sulfate (re-)cycling in the oceanic crust: Effects of seawater-rock interaction, sulfur reduction and temperature on the abundance and isotope composition of anhydrite

Barbara I. Kleine [a,*], Andri Stefánsson [a], Robert A. Zierenberg [b], Heejin Jeon [c], Martin J. Whitehouse [c], Kristján Jónasson [d], Gudmundur Ó. Fridleifsson [e], Tobias B. Weisenberger [f]

[a] *Institute of Earth Sciences, University of Iceland, Reykjavík, Iceland*
[b] *Department of Earth and Planetary Sciences, University of California at Davis, USA*
[c] *Swedish Museum of Natural History, Stockholm, Sweden*
[d] *Icelandic Institute of Natural History, Garðabær, Iceland*
[e] *Icelandic Deep Drilling Project, Garðabær, Iceland*
[f] *Research Centre Breiðdalsvík, University of Iceland, Breiðdalsvík, Iceland*

Received 16 September 2020; accepted in revised form 12 October 2021; Available online 19 October 2021

Abstract

At mid-ocean ridges (MORs), seawater carrying dissolved sulfate (SO_4) infiltrates the oceanic crust. Hydrothermal fluid emissions from such systems have much lower $\delta^{34}S$ and sulfur is mostly present as reduced sulfide, albeit in lower total sulfur concentrations than in seawater. This has been explained by anhydrite formation and sulfate reduction based on petrographic evidence and mass balance considerations. Here, we utilize the chemical and stable isotope ($\delta^{34}S$, $\delta^{18}O$) systematics in natural anhydrite and pyrite from various locations along the submarine and on-land section of the Mid-Atlantic ridge near Iceland to quantify the key variables that control anhydrite formation and sulfate recycling in the oceanic crust. Hydrothermal anhydrite exhibited $\delta^{34}S$ values of +20.6 ± 1.0‰ and $\delta^{18}O$ values between +2.4 to +25.3‰. Volcanogenic anhydrite in encrustations showed $\delta^{34}S$ values of −1.7 to +21.4‰ and $\delta^{18}O$ values between +1.4 and +38.0‰. Hydrothermal pyrite exhibited $\delta^{34}S$ values ranging from +3.4 and +19.7‰. Comparison of the natural dataset with results from geochemical isotope modelling revealed that $\delta^{34}S$ and $\delta^{18}O$ values of anhydrite and pyrite were dependent on the isotope composition of the source fluid, extent of water–rock interaction, temperature, and redox conditions. Departures of $\delta^{34}S$ and $\delta^{18}O$ values in anhydrite from the source fluid were caused by progressive fluid-basalt interaction where lower $\delta^{34}S$ and $\delta^{18}O$ values reflected a change in sources of S and O from solely fluid to basaltic origin. The $\delta^{18}O$ values of anhydrite were additionally affected by temperature. Quantitative formation of anhydrite mainly occurred at temperatures < 150 °C, whereas at elevated temperatures (>200 °C) reduction of seawater-sulfate to H_2S and subsequent pyrite precipitation were found to limit anhydrite formation. Extending our calculations to the oceanic crust revealed that the majority of seawater-sulfate is sequestered into anhydrite (3–38 Tg S yr^{-1}) in vicinity of MORs at < 200 °C at shallow depth (<1500 m), with only a small portion of seawater-derived SO_4 discharged by high-temperature hydrothermal vents (0.1–3.4 Tg S yr^{-1}). However, sequestration of sulfur by

* Corresponding author.
E-mail address: barbarak@hi.is (B.I. Kleine).

https://doi.org/10.1016/j.gca.2021.10.016

anhydrite is not long-lasting due to retrograde dissolution of anhydrite. The removal of anhydrite upon cooling and aging of the crust may result in a return back to the oceans of 10–60% of the sulfur originally sequestered in anhydrite upon hydrothermal alteration in vicinity of MORs.

Keywords: Sulfur isotopes; Oxygen isotopes; Fluid-rock interaction; Oceanic crust; Mid-Atlantic ridge; Anhydrite; Reaction path modelling

1. INTRODUCTION

Over the past decades, it has been demonstrated that subduction-related volcanic rocks contain lower sulfur contents of < 40 ppm and higher sulfur isotope ($\delta^{34}S$) values of +2.3 to +20.7‰ compared to mid-ocean ridge (MOR) basalts with sulfur contents of 800 ± 100 ppm and $\delta^{34}S$ of 0.8 ± 0.5‰ (e.g., Sasaki and Ishihara, 1979; Ueda and Sakai, 1984; Rye et al., 1984; Woodhead et al., 1987; Ishihara and Sasaki, 1989; Alt et al., 1993; Bernard et al., 1996; Imai et al., 1996; De Hoog et al., 2001; Luhr and Logan, 2002; Saal et al., 2002; Luhr, 2008). This difference between subduction-related volcanic rocks and MOR basalt has been previously explained by recycling of isotopically heavy sulfur into the mantle in the form of seawater sulfate (SO_4), hydrothermally altered crust and/or submarine sediments combined with degassing of sulfur in subaerially erupted volcanics. However, only recently it has been demonstrated that slab-derived fluids may provide insufficient sulfate to explain the oxidation of the sub-arc mantle and production of the observed positive $\delta^{34}S$ signature of volcanics in arc settings (Li et al., 2020). Yet, the contribution of various sources remains speculative due to the paucity of data from the igneous basement of the oceanic crust.

The formation of anhydrite has been shown to be critical for sulfur sequestration in the oceanic crust (Kusakabe et al., 1982; Sleep, 1991; Alt, 1995a; Alt et al., 1996; Chiba et al., 1998; Teagle et al., 1998a; Teagle et al., 1998b; Spencer, 2000; Barker et al., 2010; Craddock and Bach, 2010). Anhydrite occurs in a wide range of sedimentary, igneous and metamorphic geological settings but is best known for its large abundance in thick marine evaporite deposits (Warren, 1999; Spencer, 2000). Anhydrite has also been reported to form in fumaroles at active volcanoes, hydrothermal rift- and subduction related hydrothermal systems, magmatic-hydrothermal ore deposits (Audétat et al., 2004; Stern et al., 2007; Chambefort et al., 2008) and oceanic equivalents where anhydrite-cemented chimneys envelope submarine hydrothermal vents (Kusakabe et al., 1982; Alt and Anderson, 1991; Sleep, 1991; Alt et al., 1993; Alt, 1995a; Humphris et al., 1995; Chiba et al., 1998; Teagle et al., 1998a; Teagle et al., 1998b; Alt et al., 2010; Barker et al., 2010; Craddock and Bach, 2010; Peters et al., 2010; Alt and Shanks, 2011). Experimental studies showed that anhydrite in hydrothermal environments forms upon interaction of seawater with basalt and heating of seawater to temperatures above 120 °C (Seyfried Jr and Bischoff, 1979; Shanks III et al., 1981). Due to relatively small equilibrium sulfur isotope fractionation between aqueous SO_4 and anhydrite (Balan et al., 2014; Eldridge et al., 2016), anhydrite has often been used to track $\delta^{34}S$ variations of seawater through geological time (Paytan et al., 2004; Strauss et al., 2013; Bernasconi et al., 2017).

Although the mechanism of anhydrite formation is well understood, the largest enigma – the fate and whereabouts of anhydrite and SO_4 in the oceanic crust – remains a subject of debate. Seawater with 28.3 mmol kg^{-1} dissolved SO_4 concentration (Bruland, 1983) and $\delta^{34}S$ of +21.2‰ (Tostevin et al., 2014) infiltrates the oceanic crust in hydrothermal recharge zones at ocean ridge crests. However, hydrothermal vent fluid discharges commonly exhibit fluids with $\delta^{34}S$ of +1 to +7‰, negligible SO_4 concentration and elevated H_2S concentration typically of 4.4–8.8 mmol k g^{-1} (e.g., Von Damm et al., 1985a; Von Damm, 1995; Von Damm et al., 1995; Seal et al., 2000b; Shanks III, 2001; Lilley et al., 2003; Ono et al., 2007; McDermott et al., 2015). To account for the observed heat loss in axial hydrothermal systems, significant volumes of hydrothermal fluid must circulate through the upper crust (Sleep, 1991; Mottl and Wheat, 1994; Stein and Stein, 1994; Teagle et al., 1998b). As only insignificant amounts of SO_4 are emitted from axial hydrothermal vents, the circulating fluids must have lost almost all SO_4 by either reduction of seawater-SO_4 to H_2S, pyrite formation or extensive anhydrite formation upon seawater infiltration of the oceanic crust (Shanks III et al., 1981; McDuff and Edmond, 1982). Thereby, anhydrite deposition most likely occurred upon temperature increase or fluid mixing of cool recharge with hot discharge fluids causing potential clogging of available porosity and thus limiting further hydrothermal circulation (Seyfried Jr and Bischoff, 1979; Sleep, 1991; Teagle et al., 1998b; Lowell et al., 2003; Barker et al., 2010). Significant anhydrite deposits in the altered oceanic crust have been reported from Ocean Drilling Program (ODP) Holes 504B and 1256D in the eastern Pacific, beneath hydrothermal vent fields such as the Trans-Atlantic Geotraverse (TAG) and Logatchev on the Mid-Atlantic Ridge (MAR), from Hole 735B at the South West Indian ridge and the PACMANUS hydrothermal area in the Manus back-arc basin (Kusakabe et al., 1982; Kusakabe et al., 1989; Alt and Anderson, 1991; Chiba et al., 1998; Teagle et al., 1998a; Teagle et al., 1998b, c; Teagle et al., 2006; Alt et al., 2010; Craddock and Bach, 2010; Peters et al., 2010; Alt and Shanks, 2011). The scarcity of anhydrite from crustal samples also known as the anhydrite conundrum (Sleep, 1991; Teagle et al., 1998b) has been explained by (1) retrograde solubility of anhydrite and dissolution at lower temperature with cooling of the oceanic crust (Sleep, 1991), (2) lack of appropriate samples from the oceanic basement (Teagle et al., 1998b) and/ or (3)

a generally low hydrothermal flux in the crust leading to limited anhydrite formation during hydrothermal circulation and SO_4-bearing hydrothermal fluids diffusively returning to the ocean (Teagle et al., 1998b; Teagle et al., 2003). Thus, it remains poorly understood whether seawater circulation within the oceanic crust permanently removes SO_4 from seawater by anhydrite formation or reduction to H_2S or whether anhydrite is recycled by dissolution back to the oceans upon cooling and aging of the crust with a similar chemical and isotopic signature. Although numerous attempts have been undertaken to constrain the SO_4 flux into the oceanic crust and ridge flanks systems (e.g., Alt, 2003; Coogan et al., 2019; Staudigel, 2014; and reference therein; Teagle et al., 1998b), the chemical flux upon sulfate reduction and retrograde anhydrite dissolution remains largely unknown.

Here, we aim to constrain the SO_4 fluxes to and from the major sulfate reservoirs in the oceanic crust. For this purpose, we utilized stable isotopes ($\delta^{34}S$, $\delta^{18}O$) to identify the sources of sulfur and oxygen in anhydrite and pyrite formed in vicinity of a MOR setting. We applied geochemical isotope modelling to the dataset to assess and quantify the key variables (fluid source, extent of fluid-rock reaction, temperature, redox conditions) that control the formation and $\delta^{34}S$ and $\delta^{18}O$ systematics in anhydrite. The same modelling approach was subsequently expanded (1) to investigate the whereabouts of anhydrite and SO_4 at elevated temperatures and upon cooling of the crust and (2) estimate SO_4 chemical fluxes to and from MORs to evaluate potential SO_4 recycling into the oceans.

2. SAMPLE SET AND GEOLOGICAL SETTINGS

Anhydrite and pyrite samples were collected from a set of localities located along the MAR near to Iceland to investigate the processes that affect anhydrite formation in MOR systems (Fig. 1). Details on the geology of the sampling localities can be found in the supplementary material.

The sample set contained hydrothermal anhydrite and pyrite from drill cuttings from wells RN-10, RN-30, and RN-36 into the high-temperature (>420 °C) seawater-dominated hydrothermal system at Reykjanes (SW Iceland) to investigate anhydrite formation in hydrothermal system in vicinity of MORs. Furthermore, pyrite precipitated as scale within the production pipe of well RN-09 was included to resemble the isotopic signature of hydrothermal fluid discharge. The Reykjanes hydrothermal field is located on the southwestern tip of the Reykjanes peninsula (SW Iceland) and consists of basalt lavas and hyaloclastites that have been intruded by shallow dikes and sills (Franzson et al., 2002; Friðleifsson et al., 2020). The reservoir temperatures range from 100 °C to > 420 °C (Bali et al., 2020) and the host rocks are extensively altered by the circulating hydrothermal fluids of dominantly seawater origin (Pope et al., 2009).

Anhydrite from drill core from borehole SE-3 (Jackson et al., 2019) into the seawater-dominated hydrothermal

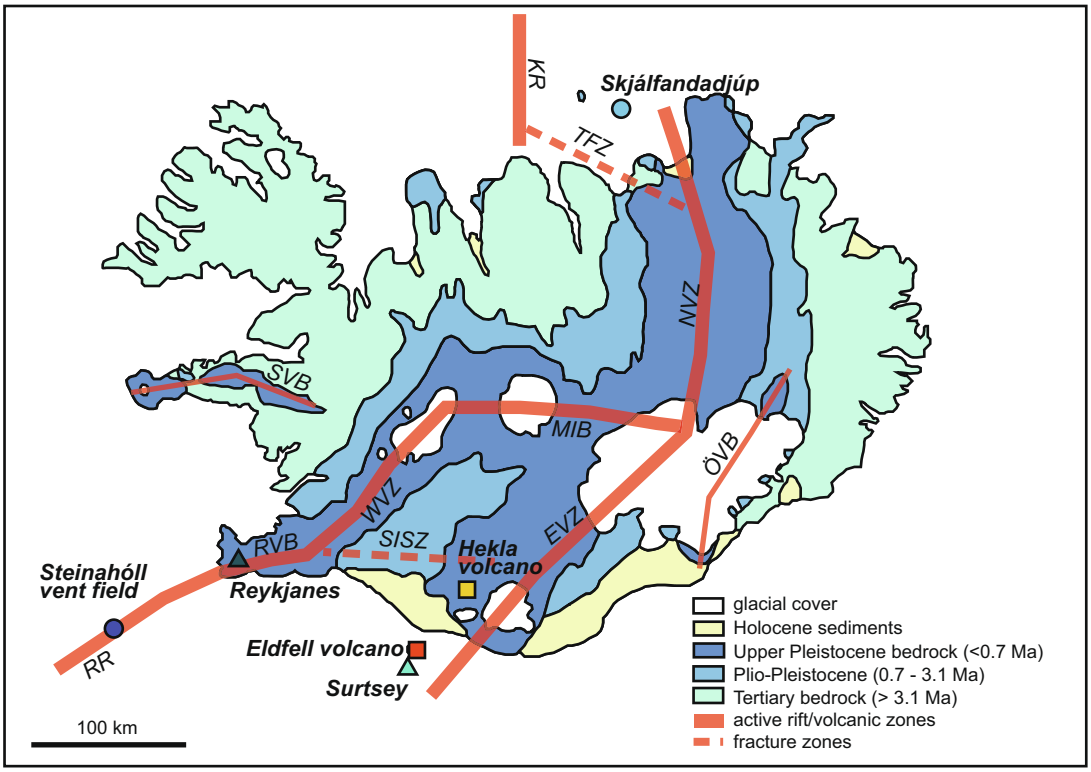

Fig. 1. Schematic map of the sample localities Reykjanes, Steinahóll vent-field, Skjálfandadjúp, Surtsey, Eldfell volcano and Hekla volcano along the submarine and on-land section of the Mid-Atlantic Ridge. RR: Reykjanes Ridge; RVB: Reykjanes Volcanic Belt; WVZ: West Volcanic Zone; MIB: Mid-Iceland Belt; SISZ: South Iceland Seismic Zone; EVZ: East Volcanic Zone; NVZ: North Volcanic Zone; TFZ: Tjörnes Fracture Zone; KR: Kolbeinsey Ridge; ÖVB: Öræfi Volcanic Belt; SVB: Snæfellsnes Volcanic Belt. Modified after Thordarson and Larsen (2007).

system at Surtsey (S Iceland) was also included to mimic conditions typical for lower temperature hydrothermal systems within the oceanic crust. The oceanic island of Surtsey grew from the seafloor during explosive and effusive eruptions from 1963 to 1967 (Thorarinsson et al., 1964). The hydrothermal system at Surtsey is hosted in tephra and tuff deposits (Jakobsson and Moore, 1986; Jackson et al., 2019; Prause et al., 2020) with hydrothermal fluid reservoir temperatures of ~ 50–140 °C (Jakobsson and Moore, 1986; Jackson et al., 2019; Kleine et al., 2020b).

The sample set also includes hydrothermal anhydrite from submarine vent systems on the Reykjanes ridge (SE Iceland) and at Skjálfandadjúp (N Iceland). Anhydrite from the Reykjanes Ridge derived from the Steinahóll vent-field, which is located at 63°06′N 250–350 m below sea level and shows the strongest signs of hydrothermal activity within the area (Ólafsson et al., 1991; German et al., 1994) with vent fluid temperatures of ~ 285 °C (Palmer et al., 1995). The hydrothermal system at Skjálfandadjúp (also Skjalfandi-deep) is mainly hosted in sediments of more than 2 km of thickness (Flóvenz and Gunnarsson, 1991; Sturkell et al., 1992) with hydrothermal fluid temperatures of ~ 250 °C (Botz et al., 1999).

Volcanogenic anhydrite, that formed upon volcanic degassing, was collected from encrustations (<100–325 °C) from three locations Eldfell, Hekla and Surtsey volcanoes (S Iceland) to investigate the effect of volcanic degassing on anhydrite formation and isotope composition. During and after the Eldfell volcano eruption in 1973 fumarolic gases formed extensive encrustations on the surface of the andesitic lava and scoria (Óskarsson, 1981). The most common phases detected in the encrustations were anhydrite, opal, ralstonite (Na-Mg-Al hydrate), gypsum and hematite, followed by bassanite (calcium sulfate hydrate), jarosite ($K\text{-}Fe^{+III}$ sulfate), sulfur and sylvite, and formed at ~ 230–260 °C (Jakobsson et al., 2008). At Surtsey, encrustations formed on the surface of lava and scoria at 135 °C during the effusive phase of the Surtsey volcano eruption. They were composed of mainly gypsum, opal, calcite, fluorite, halite, ralstonite, thenardite (sodium sulfate), anhydrite and hematite (Jakobsson et al., 2008). Encrustation samples from the Hekla volcano eruptions in 1947–1948 and 1991–1993 were also included in this study. The encrustations formed upon extensive degassing at temperatures between ~ 100 and 325 °C and contained anhydrite, ralstonite, fluorite, opal, mallardite (manganese sulfate), hematite, thernadite and gypsum (Jakobsson et al., 2008).

3. METHODS

3.1. Sample processing and analysis

Five to ten anhydrite and pyrite grains (<500 μm) per sample were embedded in epoxy along with the anhydrite and pyrite reference materials, Anhydrite 1 (Reuschel et al., 2012; $\delta^{18}O = +8.42‰$ determined in this study, see Supplement A for details), Anhydrite 2 (Reuschel et al., 2012; $\delta^{34}S = +10.50‰$) and Ruttan pyrite ($\delta^{34}S = +1.41‰$, (Cabral et al., 2013)). Thereafter, the sample mount was polished using 1 μm diamond paste, and carbon coated.

The chemical composition of anhydrite (Ca, S, Sr, Ba, Mg, Pb) and pyrite (Fe, S, As, Pb, Co, Zn, Cu, Ni) were determined using a JEOL JXA-8230 electron microprobe (EMP) equipped with a LaB6 electron emitter at the University of Iceland. JEOL PC-EMPA application was used and running conditions were 15 keV accelerating voltage and 100nA cup current with a beam diameter of 1 to 10 μm. The CITZAF program (Armstrong, 1991) was used for data correction.

Oxygen and sulfur isotope ratios were determined *in-situ* using a CAMECA IMS-1280 at the NordSIMS laboratory of the Swedish Museum of Natural History. Prior to secondary ion mass spectrometry (SIMS) analysis, the carbon-coating used for the EMP analyses was removed from the sample mounts, which then were lightly re-polished (to ca. 1 μm) and gold-coated (30 nm). The isotope ratios for sulfur and oxygen are reported relative to V-CDT and V-SMOW, respectively, in the standard delta notation, $\delta^{34}S$ and $\delta^{18}O$, respectively. A $^{133}Cs^{+}$ primary beam with impact energy of 20 kV and current of 1 nA (pyrite) or 2.5 nA (anhydrite) was used to sputter secondary ions from the sample surface. A small raster (10 μm) was used throughout the analysis to homogenize the critically focused beam. A low-energy normal incidence electron gun was employed for charge compensation while measuring anhydrite. Following pre-sputtering to remove Au coat, secondary ions (^{16}O and ^{18}O; ^{32}S and ^{34}S) from the target sample were admitted to the mass spectrometer with a field magnification of ca. 90×, with automated centering of the secondary beam in the field aperture. The magnetic field was locked with high precision using an NMR field sensor. The secondary ions were simultaneously detected by Faraday Cups using amplifiers with 10^{10} Ω and 10^{11} Ω resistors at a mass resolution of ca. 2500 (M/ΔM) in a multicollection mode. Data were collected during 12 integration cycles, each with a counting time of 4 s. Typical signal intensities are ca. 3.5×10^8 counts per second (cps) for ^{32}S (anhydrite), ca. 4.0×10^9 cps for ^{16}O (anhydrite) and ca. 7.0×10^8 cps for ^{32}S (pyrite). Analyses of reference materials bracketed every six unkowns, in order to correct for drift and instrumental mass fractionation. External reproducibility (1 std. dev.) of ca. ± 0.35‰ for $\delta^{18}O$ and ca. ± 0.15‰ for $\delta^{34}S$ in anhydrite, and ca. ± 0.20‰ for $\delta^{34}S$ in pyrite was propagated onto within-run uncertainties.

In addition, pyrite precipitated as scale in the production pipe of well RN-09 and additional hydrothermal pyrite from well RN-10 at Reykjanes were analyzed using conventional gas isotope ratio mass spectrometry using the methods described in Shipp and Zierenberg (2008). Values are reported relative to the V-CDT standard. The precision of the $\delta^{34}S$ analyses based on repeated analyses of laboratory working standards is typically ± 0.3‰.

3.2. Geochemical isotope modelling

Variations in the stable isotope composition of natural anhydrite and pyrite depend on a variety of equilibrium and kinetically controlled processes including water–rock interaction, oxidation, reduction and physical parameters such as temperature, redox conditions, fluid source (Seal

et al., 2000a). Geochemical isotope modelling was carried out to investigate the effect of these factors and processes on the $\delta^{34}S$ and $\delta^{18}O$ composition of hydrothermal and volcanogenic anhydrite and pyrite.

Four scenarios were investigated: (1) anhydrite formation upon heating of seawater by either conductive heat exchange or mixing of a hydrothermal fluid; (2) seawater-basalt interaction over a range of temperature and water–rock ratios; (3) reduction of seawater-SO_4 to form pyrite as well as the reverse process of pyrite oxidation; (4) magmatic gas interaction with basalt and formation of volcanogenic anhydrite encrustations. The geochemical isotope modelling included Rayleigh modelling (Ohmoto and Goldhaber, 1997) and reaction modeling carried out with the aid of the PHREEQC program and the databases llnl.dat at > 200 °C and wateq4f.dat at < 200 °C (Parkhurst and Appelo, 1999), and the IsoGem program (Stefánsson et al., 2017a; Gunnarsson-Robin et al., 2018). The input parameters for our modelling approach such as fluid and rock chemical and isotopic compositions, and equilibrium solubility constants and isotope fractionation factors as a function of temperature are listed in Tables A1-A3. Further details on the calculations are given in Supplement A.

Anhydrite formation upon conductive heating of seawater was calculated from equilibrium solubility of anhydrite as a function of temperature without consideration of progressive basalt-seawater interaction. For these calculations, anhydrite was the only Ca and SO_4 bearing mineral considered to form. The same calculations were carried out to simulate heating of seawater through mixing of cold seawater (2 °C) with a hot (300 °C) hydrothermal fluid.

Seawater-basalt interaction was simulated using reaction path (titration) modeling over a range of temperatures (10–300 °C) and water–rock ratios (i.e., ξ the reaction progress or extent of reaction measured as the disappearance or appearance of a chemical component in a reaction) to simulate the formation of anhydrite in seawater-dominated hydrothermal systems. Unaltered basaltic rock was allowed to react in steps with seawater and saturated secondary minerals in each step were allowed to precipitate. The secondary minerals included in the calculations were those commonly observed in seawater-dominated hydrothermal systems (e.g., Alt et al., 1996; Franzson et al., 2002; Marks et al., 2011; Marks et al., 2010) and comprised actinolite, anhydrite, calcite, gibbsite, goethite, pyrite, pyrrhotite, quartz, Al-Si clays (allophane), Mg-Fe clays (saponite, nontronite), prehnite, celadonite, zeolites (chabazite, laumontite, wairakite, analcime), albite, microcline, epidote and Fe-Mg chlorite. Allowing epidote or Fe^{+III}-bearing clays to form when saturated was necessary to simulate reduction of SO_4 to sulfide (S^{-II}) as this process is commonly accompanied by the formation of Fe^{+III}-bearing mineral species (Barker et al., 2010). Following reaction modelling carried out with PHREEQC, the obtained mole fractions of various aqueous species and minerals were used to calculate sulfur and oxygen isotopes ratios for the respective aqueous species and minerals using IsoGem (Stefánsson et al., 2017a; Gunnarsson-Robin et al., 2018). The calculated isotope composition of fluids, secondary minerals and rocks is thereby dependent on the mole fractions of individual S and O containing aqueous species (H_2O, SO_4^{2-}, HS^-, H_2S, $SO_{2(aq)}$, SO_3^{2-}) and minerals (anhydrite, pyrite, celadonite, zeolite, clay, calcite, chlorite, quartz, epidote, prehnite), and equilibrium isotope fractionation between aqueous species and alteration minerals. All these factors in turn depend on temperature and extent of fluid-rock reaction, as well as pH and redox state of the reacting fluid. Details on the calculations and equilibrium isotope fractionation factors are described in Supplement A.

Reduction of seawater-SO_4 and formation of pyrite as well as pyrite oxidation were simulated by applying a Rayleigh model (Ohmoto and Goldhaber, 1997) to investigate equilibrium and kinetic effects on stable isotope variations measured in pyrite and anhydrite. An open system type Rayleigh model was assumed for both reduction and oxidation processes, where the back reaction is non-reactive. Here, we calculated the Rayleigh distillation curves for abiotic reduction of seawater-SO_4 and oxidation of pyrite showing the change in $\delta^{34}S$ of H_2S, SO_4, anhydrite and pyrite as a function of reaction progress. Reduction is a likely process to occur at elevated temperatures (>200 °C) in seawater-dominated hydrothermal systems, where chemical and isotopic equilibrium is attained between sulfide and sulfate (Ohmoto and Lasaga, 1982). The $\delta^{34}S$ values of anhydrite and pyrite were thus calculated using equilibrium isotope fractionation values of mineral-SO_4 pairs from the temperature dependent equations given in Table A3. Oxidation of pyrite at < 150 °C may lead to an $\delta^{34}S$ enrichment of up to 5‰ in the forming aqueous sulfate and soluble sulfate mineral relative to the initial isotope value of the pyrite (Taylor and Wheeler, 1994; Ohmoto and Goldhaber, 1997; Budakoglu and Pratt, 2005; Lefticariu et al., 2006). For the simulation of anhydrite formation upon pyrite oxidation, we chose non-equilibrium enrichment factors of $\alpha_{SO4\text{-}py} = 1.0005$ for the SO_4-pyrite pair and $\alpha_{anh\text{-}py} = 1.0008$ for the anhydrite-pyrite pair which correspond to enrichment factors of 0.5‰ and 0.8‰, respectively. Such low enrichment values relative to pyrite are common and have been reported by Lefticariu et al. (2006) for aqueous SO_4 and anhydrite, respectively.

Interaction between magmatic gas and basalt and associated formation of volcanogenic anhydrite encrustations was simulated using reaction path (titration) model with the aid of PHREEQC and IsoGem programs in a similar manner as for the seawater-basalt interaction calculations. Thereby, unaltered rock was allowed to react with a condensed magmatic gas of a chemical composition typical for volcanic gasses emitted from Icelandic volcanoes (Sigvaldason and Elísson, 1968; Stefánsson et al., 2017b; Ilyinskaya et al., 2018). Anhydrite was the only mineral allowed to precipitate when saturated. The $\delta^{18}O$ and $\delta^{34}S$ isotope composition of major fluid species (H_2O, SO_4^{2-}, H_2S, HS^-), anhydrite and pyrite as well other secondary minerals was calculated using mole fractions retrieved from the reaction path model and equilibrium isotope fractionation between aqueous species and alteration minerals. Details on the calculations are given in Supplement A. The initial isotope values and chemical composition of fluids and rocks used in the model are given in Table A1. Equilibrium isotope fractionation factors used to calculate

the isotope composition of fluid species and minerals are listed in Table A3.

Although the reaction path model requires system equilibrium, exchange kinetics between SO_4 and H_2S are very slow at temperatures < 200 °C and equilibrium in the system cannot be assumed (Ohmoto and Lasaga, 1982). However, at such low temperatures the reduction of SO_4 to H_2S is limited in seawater-dominated hydrothermal systems and therefore the influence of H_2S production on the isotopic composition of seawater is insignificant because of mass balance.

Note, that this geochemical model focuses only on the chemical aspects of hydrothermal activity in the crust while greatly simplifying the reservoir physics of such systems. Fluid flow dynamics and chemical transport drive the interaction between water and host rocks, however, complex hydrothermal processes leading to the formation of anhydrite cannot yet successfully be computed by reactive transport and numerical modelling approaches (Sleep, 1991; Alt-Epping and Diamond, 2008).

4. RESULTS

4.1. Chemical and isotopic composition of anhydrite and pyrite

Anhydrite from all samples was observed to be of almost pure endmember composition ($CaSO_4$) and only contained minor amounts of Sr (580–2570 ppm), Mg (230–3550 ppm) and Ba (120–1040 ppm). Pyrite (FeS_2) contained minor impurities of As (250–1890 ppm), Pb (1020–1370 ppm) and Zn (130–490 ppm) (Tables A5 and A6, Fig. A1).

The isotope composition of anhydrite and pyrite displayed wide and irregular ranges (Tables 1 and 2; Fig. 2). Hydrothermal anhydrite from submarine vent systems at Steinahóll at the Reykjanes ridge and Skjálfandadjúp showed $\delta^{18}O$ values of +7.8 ± 1.8‰ and $\delta^{34}S$ values of +21.1 ± 0.6‰. The $\delta^{18}O$ and $\delta^{34}S$ values of anhydrite from the hydrothermal system at Surtsey (~50–140 °C) clustered at +8.9 ± 4.5‰ and +19.2 ± 0.5‰, respectively. The $\delta^{18}O$ and $\delta^{34}S$ values of anhydrite from the hydrothermal system at Reykjanes (~100 °C to > 420 °C) differed slightly and clustered at +7.2 ± 1.6‰ and +20.4 ± 1.1‰, respectively. Hydrothermal pyrite from Reykjanes collected from drill cuttings showed $\delta^{34}S$ values ranging from +3.4 to +19.7‰. The $\delta^{34}S$ values of pyrite and sulfate precipitated within the production pipe of well RN-09 clustered at +3.0 ± 0.6‰ and +2.9 ± 0.6‰, respectively. The isotope composition of volcanogenic anhydrite spanned over a large range with $\delta^{18}O$ of +1.4 to +38.0‰ and $\delta^{34}S$ of −1.6 to +21.4‰.

4.2. Geochemical isotope modelling

4.2.1. Heating of seawater and associated anhydrite formation

Heating of seawater and associated anhydrite formation by either conductive heat exchange or mixing of cold seawater with hot hydrothermal fluids are common processes occurring in vicinity to hydrothermal vents (e.g., Skikazono et al., 1983; Teagle et al., 1998a; Teagle et al., 1998b; Teagle et al., 1998c; Lowell et al., 2003; Kawada and Yoshida, 2010). Due to retrograde solubility, anhydrite may form when seawater is heated to above 120 °C (Seyfried Jr and Bischoff, 1979), where Ca and SO_4 are both sourced from seawater. Equilibrium sulfur and oxygen isotope fractionation between anhydrite and seawater is positive (Zeebe, 2010; Balan et al., 2014; Eldridge et al., 2016), resulting in the enrichment of the ^{34}S and ^{18}O in the solid phase. With progressive heating of seawater to 300 °C sulfur and oxygen isotope fractionation between anhydrite and the fluid phase decreases and approximates 0‰. Thus, during conductive heating the $\delta^{34}S$ of anhydrite was predicted to approach the isotope values of seawater. The $\delta^{18}O$ values of anhydrite approached the $\delta^{18}O$ value of seawater-SO_4 (+9.6‰ (Kusakabe et al., 1982)) with increasing temperature and subsequently decreased below the seawater value above about 210 °C (Figs. A3). Heating of cold seawater (2 °C) by mixing with a hot hydrothermal fluid (300 °C) resulted in slightly lower $\delta^{34}S$ values in precipitating anhydrite (Fig. 3). This is because $\delta^{34}S$ in anhydrite might derive partly from the hydrothermal fluid that commonly exhibit lower $\delta^{34}S$ values with respect to seawater. At temperature > 200 °C, reduction inhibits anhydrite formation which results in residual SO_4 becoming slightly more ^{34}S-enriched relative to seawater due to the incorporation of ^{32}S into the forming sulfide species.

4.2.2. Seawater-basalt interaction at 10–300 °C

The simulation of fluid-rock interaction and associated sulfur reduction as a function of temperature and extent of reaction was carried out to reproduce the processes that affect the formation of hydrothermal anhydrite and pyrite and their isotopic composition upon seawater-basalt interaction at 10–300 °C.

With progressive fluid-rock interaction, the model predicted a shift in the source fraction of sulfur and oxygen. The shift from a seawater- to a rock-dominated sulfur and oxygen source in anhydrite and pyrite was reflected in the calculated $\delta^{18}O$ and $\delta^{34}S$ values over the extent of seawater-rock reaction (Fig. 4). With progressive seawater-rock reaction, both $\delta^{18}O$ and $\delta^{34}S$ values of anhydrite and pyrite approached the isotope value of unaltered basalt. At low temperature (<150 °C), the formation of anhydrite was the primary process that limited sulfur concentrations in the reacted and hydrothermally modified seawater. The model predicted that with progressive reaction of basalt, increasing amounts of sulfide (S^{-II}) was released from the basalt into the solution resulting in HS^- and H_2S eventually becoming the dominant aqueous sulfur species in the solution at $\xi = 0.1$ mol basalt dissolved in 1 kg seawater (Fig. 3). At higher temperatures (>200 °C), epidote was predicted to form in significant amounts (>0.1 mol kg^{-1}) initiated by the oxidation of Fe^{+II} to Fe^{+III} upon progressive basalt alteration. Oxidation of Fe^{+II} was coupled with the reduction of SO_4 to H_2S leading to increased dissolved sulfide concentrations and eventually to the formation of pyrite at elevated temperatures.

Table 1
Isotopic composition of anhydrite from Reykjanes, Surtsey, Reykjanes ridge, Skjálfandadjúp, Eldfell, and Hekla. Presented values are the average values of five grains analyzed and the error represents 1 std. The $\delta^{18}O$ and $\delta^{34}S$ values are reported relative to V-SMOW and V-CDT, respectively.

Sample-ID	Location	Grain #	Depth (m)	$\delta^{18}O$	±	$\delta^{34}S$	±
				‰		‰	
Hydrothermal anhydrite							
RN-734	Reykjanes (RN-36)	1	734	7.2	0.4	19.9	0.1
RN-734		2	734	6.9	0.4	19.8	0.1
RN-734		3	734	7.3	0.4	20.6	0.1
RN-734		4	734	7.8	0.4	19.8	0.1
RN-734		5	734	6.9	0.4	19.8	0.1
RN-734		6	734	5.8	0.4	19.3	0.1
RN-734		7	734	5.5	0.4	19.8	0.2
RN-734		8	734	6.8	0.4	19.9	0.1
RN-734		9	734	6.8	0.4	19.6	0.1
RN-734		10	734	6.7	0.4	19.5	0.1
RN-752	Reykjanes (RN-36)	1	752	6.5	0.4	19.7	0.1
RN-752		2	752	7.1	0.4	20.3	0.1
RN-752		3	752	7.4	0.4	20.5	0.1
RN-752		4	752	5.9	0.4	20.3	0.1
RN-752		5	752	6.5	0.4	19.1	0.1
RN-752		6	752	5.7	0.4	19.5	0.1
RN-752		7	752	5.3	0.4	19.8	0.1
RN-752		8	752	6.0	0.4	19.2	0.2
RN-752		9	752	4.9	0.4	19.4	0.1
RN-1466	Reykjanes (RN-30)	1	1466	9.5	0.3	21.5	0.2
RN-1466		2	1466	9.9	0.3	21.4	0.2
RN-1466		3	1466	8.9	0.3	21.4	0.2
RN-1466		4	1466	9.7	0.3	20.3	0.2
RN-1466		5	1466	10.0	0.3	21.6	0.2
RN-1466		6	1466	5.4	0.3	21.4	0.2
RN-1466		7	1466	8.6	0.3	21.0	0.2
RN-1466		8	1466	8.5	0.3	20.9	0.2
RN-1466		9	1466	10.4	0.3	24.7	0.2
D-40	Surtsey (SE-3)	1	100	12.9	0.4	18.4	0.1
D-40		2	100	25.3	0.4		
D-82	Surtsey (SE-3)	1	200	7.2	0.4	19.6	0.1
D-82		2	200	6.4	0.4	19.2	0.1
D-82		3	200	6.4	0.4	19.2	0.1
D-82		4	200	10.1	0.4	19.4	0.1
D-82		5	200	6.8	0.4	19.0	0.2
D-82		6	200	7.2	0.4	19.0	0.1
D-82		7	200	11.7	0.4	20.9	0.2
D-82		8	200	7.2	0.4	19.0	0.1
D-82		9	200	6.3	0.4	19.6	0.2
D-82		10	200	7.4	0.4	19.5	0.2
D-94	Surtsey (SE-3)	1	230	6.0	0.4	18.4	0.1
D-94		2	230	6.0	0.4	19.4	0.2
D-94		3	230	5.5	0.4	18.8	0.2
D-103	Surtsey (SE-3)	1	250	6.3	0.4	19.6	0.1
D-116	Surtsey (SE-3)	1	280	10.0	0.4	19.2	0.1
D-116		2	280	9.9	0.4	19.2	0.1
D-116		3	280	10.3	0.4	19.3	0.1
D-116		4	280			19.3	0.1
Hydrothermal anhydrite from submarine vents							
NI-13605	Reykjanes ridge	1	0	8.2	0.3	20.1	0.2
NI-13605		2	0	8.3	0.3	20.8	0.2
NI-13605		3	0	6.6	0.3	20.4	0.2
NI-13605		4	0	8.7	0.3	19.7	0.2
NI-13605		5	0	6.5	0.3	20.7	0.2
NI-13605		6	0	7.2	0.3	21.2	0.2
NI-13605		7	0	8.0	0.3	19.9	0.2
NI-13605		8	0	5.1	0.3	20.1	0.2

(*continued on next page*)

Table 1 (*continued*)

Sample-ID	Location	Grain #	Depth (m)	$\delta^{18}O$	±	$\delta^{34}S$	±
				‰		‰	
NI-13605		9	0	7.2	0.3	20.4	0.2
NI-13605		10	0	6.9	0.3	21.4	0.2
NI-13602	Skjálfandadjúp	1	0	8.1	0.3	21.0	0.2
NI-13602		2	0	2.7	0.3	21.3	0.2
NI-13602		3	0	7.6	0.3	20.8	0.2
NI-13602		4	0	8.9	0.3	22.7	0.2
NI-13602		5	0	8.5	0.3	21.5	0.2
NI-13602		6	0	7.5	0.3	21.6	0.2
NI-13602		7	0	3.3	0.3	21.1	0.2
NI-13602		8	0	3.2	0.4	20.7	0.2
NI-13602		9	0	2.4	0.3	20.6	0.2
NI-13602		10	0	3.0	0.3	20.9	0.2
NI-13603	Skjálfandadjúp	1	0	5.7	0.3	21.6	0.2
NI-13603		2	0	9.4	0.3	21.8	0.2
NI-13603		3	0	6.5	0.3	21.6	0.2
NI-13603		4	0	7.4	0.3	20.0	0.2
NI-13603		5	0	7.7	0.3	20.3	0.2
NI-13603		6	0	7.5	0.3	20.8	0.2
NI-13603		7	0	10.2	0.3	21.1	0.2
NI-13603		8	0	10.1	0.3	21.8	0.2
NI-13603		9	0	7.0	0.3	21.2	0.2
NI-13603		10	0	9.8	0.3	20.2	0.2
NI-13604	Skjálfandadjúp	1	0	9.0	0.3	21.6	0.2
NI-13604		2	0	9.0	0.3	21.5	0.2
NI-13604		3	0	9.6	0.3	21.8	0.2
NI-13604		4	0	9.9	0.3	21.0	0.2
NI-13604		5	0	8.4	0.3	21.2	0.2
NI-13604		6	0	8.8	0.3	21.1	0.2
NI-13604		7	0	8.6	0.3	21.3	0.2
NI-13604		8	0	8.6	0.3	21.3	0.2
NI-13604		9	0	9.1	0.3	21.4	0.2
NI-13604		10	0	9.9	0.3	22.1	0.2
NI-15504	Skjálfandadjúp	1	0	8.6	0.3	21.7	0.2
NI-15504		2	0	8.1	0.3	21.7	0.2
NI-15504		3	0	8.1	0.3	21.7	0.2
NI-15504		4	0	8.5	0.3	21.3	0.2
NI-15504		5	0	8.6	0.3	21.5	0.2
NI-15504		6	0	8.6	0.3	21.6	0.2
NI-15504		7	0	8.2	0.3	21.5	0.2
NI-15504		8	0	8.8	0.3	21.3	0.2
NI-15504		9	0	9.0	0.3	21.3	0.2
NI-15504		10	0	8.2	0.3	21.6	0.2
NI-15525	Skjálfandadjúp	1	0	8.1	0.3	21.0	0.2
NI-15525		2	0	7.3	0.3	21.2	0.2
NI-15525		3	0	8.4	0.3	21.0	0.2
NI-15525		4	0	8.4	0.3	21.0	0.2
NI-15525		5	0	8.3	0.3	21.0	0.2
NI-15525		6	0	8.6	0.3	21.1	0.2
NI-15525		7	0	8.6	0.3	20.9	0.2
NI-15525		8	0	8.1	0.3	20.8	0.2
NI-15525		9	0	9.2	0.3	20.9	0.2
NI-15525		10	0	8.5	0.3	21.1	0.2
Vulcanogenic anhydrite encrustations							
NI-12251	Eldfell	1	surface	35.3	0.3	3.7	0.2
NI-12251		2		38.0	0.3	3.0	0.2
NI-12251		3		37.5	0.3	3.3	0.2
NI-12251		4		36.3	0.3	3.0	0.2
NI-12251		5		36.7	0.3	3.8	0.2
NI-13561	Eldfell	1	surface	12.3	0.4	−1.0	0.2
NI-13561		2		13.2	0.4	−0.1	0.2

(*continued on next page*)

Table 1 (*continued*)

Sample-ID	Location	Grain #	Depth (m)	$\delta^{18}O$	±	$\delta^{34}S$	±
				‰		‰	
NI-13561		3		13.3	0.4	−0.5	0.2
NI-13561		4		13.7	0.3	−1.5	0.2
NI-13561		5		13.4	0.3	−0.5	0.2
NI-13561		6		12.9	0.3	0.6	0.2
NI-13561		7		14.8	0.3	−0.6	0.2
NI-13561		8		12.7	0.3	−0.4	0.2
NI-13561		9		14.4	0.3	−0.4	0.2
NI-20624	Eldfell	1	0.3	8.9	0.3	21.3	0.2
NI-20624		2				7.1	0.2
NI-20624		3		14.0	0.3		
NI-20624		4		12.3	0.3	6.8	0.2
NI-20624		5		11.5	0.3	9.2	0.2
NI-20624		6		10.9	0.4		
NI-12389	Surtsey	1	surface	8.0	0.3	21.2	0.2
NI-12389		2		8.4	0.3	21.1	0.2
NI-12389		3		7.1	0.3	21.2	0.2
NI-12389		4		7.9	0.3	21.2	0.2
NI-12389		5		7.1	0.3	21.3	0.2
NI-12389		6		7.8	0.3	21.2	0.2
NI-12389		7		7.3	0.3	21.4	0.2
NI-12389		8		7.9	0.3	21.1	0.2
NI-12389		9		7.7	0.3	21.1	0.2
NI-12389		10		7.4	0.3	21.3	0.2
NI-15969	Hekla	1	surface	8.8	0.4		
NI-15969		2		8.3	0.3		
NI-15969		3		6.0	0.3	10.9	0.2
NI-15969		4		4.3	0.3		
NI-15969		5		7.7	0.3	20.6	0.2
NI-17062	Hekla	1	0.8	7.6	0.3	5.3	0.2
NI-17062		2		4.4	0.3		
NI-17062		3		9.0	0.3	2.9	0.2
NI-17062		4		4.6	0.3	3.6	0.2
NI-17062		5		2.5	0.3	2.2	0.2
NI-17062		6		1.4	0.3	3.3	0.2
NI-17062		7		6.7	0.3	2.4	0.2
NI-17062		8		10.7	0.3		
NI-17062		9		12.4	0.3	2.2	0.2

4.2.3. Reduction of seawater-SO_4 and oxidation of pyrite

The effect of seawater-SO_4 reduction and the formation and $\delta^{34}S$ values of pyrite and residual anhydrite at elevated temperatures (>200 °C) was qualitatively constrained using a Rayleigh-type model (Ohmoto and Goldhaber, 1997) and quantitatively constrained using the reaction (titration) model for seawater-basalt interaction. The reaction model revealed that reduction of SO_4 to H_2S upon progressive basalt alteration is initiated by the hydrolysis of aqueous Fe^{+II} to aqueous Fe^{+III} species and subsequent formation of epidote at > 200 °C and pH > 9. The oxidation of Fe^{+II} to Fe^{+III} was thereby found to be accompanied by reduction of SO_4 to H_2S and H_2O to H_2. Such redox reactions as observed for the basalt-seawater system studied here, may be common in seawater-dominated hydrothermal systems and have been previously reported to occur upon reaction of basaltic oceanic crust with oxygenated seawater and associated formation of Fe^{+III}-bearing Fe-oxyhydroxides, smectite and celadonite (Honnorez, 1981; Alt, 1995b). The product H_2S may further precipitate as pyrite via reaction with Fe^{+II}-bearing (chlorite, amphibole) or Fe^{+III}-bearing minerals (epidote, hematite) and/or reaction with Fe^{+II} leached from the host rock into the reacted solution upon progressive fluid-rock interaction.

The Rayleigh model revealed that progressive SO_4 reduction would lead to the gradual ^{34}S-enrichment of the residual SO_4 resulting in progressively more positive $\delta^{34}S$ ratios of dissolved SO_4 and anhydrite (Fig. 5) relative to seawater. Due to fractionation between sulfate and sulfide bearing minerals and fluid species, the $\delta^{34}S$ values of pyrite precipitated from H_2S were significantly less positive than the isotope value of the residual SO_4.

Oxidation of sulfides (e.g., pyrrhotite, pyrite) in the oceanic crust commonly occurs throughout the igneous crust over a broad temperature range (Seal et al., 2000a). Sulfur isotope fractionation between dissolved sulfate and sulfate mineral and the residual sulfide mineral ($\alpha_{sulfate\text{-}sulfide}$) is small or < 1.005 even at low temperatures (<150 °C) (Taylor and Wheeler, 1994; Ohmoto and Goldhaber, 1997; Budakoglu and Pratt, 2005; Lefticariu

Table 2
Isotopic composition of hydrothermal pyrite from well RN-10 and pyrite and sulfate precipitated in the production pipes as scale from well RN-09 at Reykjanes. Presented values are the average values of five grains analyzed and the error represents 1 std. Values are reported relative to V-CDT.

Sample-ID	Depth (m)	Distance from wellhead (m)	Analytical method	$\delta^{34}S$	±
				‰	
Hydrothermal pyrite from drill cuttings (well RN-10)					
RN100	100		(1)	3.4	0.0
RN550	550		(1)	5.7	0.0
RN760	760		(1)	18.5	0.9
RN900	900		(1)	19.7	0.1
RN950	950		(1)	18.0	0.0
RN1041	1041		(2)	5.2	0.3
RN1060	1060		(2)	10.5	0.3
RN1060	1060		(2)	10.7	0.3
RN1110	1110		(1)	4.6	0.7
RN1140	1140		(2)	4.4	0.3
RN1140	1140		(2)	5.1	0.3
RN1140	1140		(2)	6.6	0.3
RN1182	1182		(2)	7.9	0.3
RN1182	1182		(2)	8.0	0.3
RN1182	1182		(2)	5.9	0.3
RN1230	1230		(2)	6.4	0.3
RN1260	1260		(1)	9.8	0.2
RN1350	1350		(1)	6.4	0.0
RN1400	1400		(1)	5.1	0.8
RN1450	1450		(1)	7.4	1.6
RN1500	1500		(1)	5.5	0.0
RN1522	1522		(2)	9.0	0.3
RN1522	1522		(2)	9.3	0.3
RN1522	1522		(2)	6.6	0.3
RN1550	1550		(1)	6.7	0.1
RN1650	1650		(1)	6.2	0.0
RN1700	1700		(1)	6.4	0.1
RN1702	1702		(2)	6.2	0.3
RN1702	1702		(2)	6.1	0.3
RN1800	1800		(1)	6.7	0.1
RN1850	1850		(1)	6.8	0.6
RN1900	1900		(1)	4.5	0.3
RN1948	1948		(2)	4.8	0.3
RN1948	1948		(2)	5.1	0.3
RN1950	1950		(1)	7.2	0.1
RN1996	1996		(2)	4.9	0.3
RN2026	2026		(2)	4.8	0.3
RN2026	2026		(2)	9.3	0.3
Pyrite and sulfate precipitated as scales (well RN-09)					
9RN08_2001 pyrite		−1	(2)	3.8	0.3
9RN08_2001 sulfate		−1	(2)	3.7	0.3
9RN09 pyrite		1	(2)	3.8	0.3
9RN21_A pyrite		11	(2)	3.4	0.3
9RN21_A sulfate		11	(2)	2.7	0.3
9RN31 A pyrite		12	(2)	3.3	0.3
9RN31 B pyrite		12	(2)	2.7	0.3
9RN19 pyrite		13	(2)	2.8	0.3
9RN18 A pyrite		13	(2)	3.1	0.3
9RN17 pyrite		13	(2)	2.8	0.3
9RN17 K pyrite		13	(2)	2.7	0.3
9RN17 sulfate		13	(2)	2.9	0.3
9RN16 pyrite		13	(2)	3.0	0.3
9RN29 A pyrite		17	(2)	3.1	0.3
9RN29 B Cp pyrite		17	(2)	2.5	0.3
9RN29 C pyrite		17	(2)	2.4	0.3
9RN29 D pyrite		17	(2)	2.7	0.3

(*continued on next page*)

Table 2 (*continued*)

Sample-ID	Depth (m)	Distance from wellhead (m)	Analytical method	$\delta^{34}S$	±
				‰	
9RN29 E pyrite		17	(2)	2.4	0.3
9RN29 E sulfate		17	(2)	2.1	0.3
9RN27 A pyrite		18	(2)	2.8	0.3
9RN27 B pyrite		18	(2)	2.9	0.3
9RN27 C pyrite		18	(2)	2.9	0.3
9RN27 E pyrite		18	(2)	2.6	0.3
9RN27 F pyrite		18	(2)	2.9	0.3
9RN27 G pyrite		18	(2)	3.0	0.3
9RN27 H pyrite		18	(2)	2.8	0.3
9RN27 I pyrite		18	(2)	3.2	0.3
9RN27 J pyrite		18	(2)	3.3	0.3
9RN27 K sulfate		18	(2)	3.3	0.3
9RN1 A pyrite		20	(2)	2.7	0.3
9RN1 B pyrite		20	(2)	2.9	0.3
9RN1 C pyrite		20	(2)	2.8	0.3
9RN1 D pyrite		20	(2)	2.7	0.3
9RN1 E pyrite		20	(2)	2.8	0.3
9RN26 BASE C pyrite		24	(2)	2.9	0.3
9RN26 BASE C sulfate		24	(2)	2.5	0.3
9RN26 TOP C pyrite		24	(2)	2.7	0.3
9RN26 TOP D pyrite		24	(2)	2.9	0.3
9RN5-A pyrite		53	(2)	2.5	0.3
9RN5-A pyrite		53	(2)	2.6	0.3
9RN5-B pyrite		53	(2)	2.5	0.3
9RN5-C pyrite		53	(2)	2.4	0.3
9RN5-D pyrite		53	(2)	2.5	0.3
9RN5-E pyrite		53	(2)	2.7	0.3
9RN5-F pyrite		53	(2)	2.5	0.3
9RN7A pyrite		60	(2)	3.7	0.3
9RN6-A pyrite		85	(2)	2.8	0.3
9RN6-B pyrite		85	(2)	3.7	0.3
9RN6-B pyrite		85	(2)	3.3	0.3
9RN6-B pyrite		85	(2)	4.0	0.3
9RN6-C pyrite		85	(2)	4.1	0.3
9RN6-D pyrite		85	(2)	3.9	0.3
9RN6-D pyrite		85	(2)	2.8	0.3
9RN11-A pyrite		360	(2)	4.5	0.3
9RN13 pyrite		360	(2)	4.2	0.3
9RN13 pyrite		360	(2)	3.2	0.3
9RN14 pyrite		360	(2)	3.2	0.3
9RN15 pyrite		360	(2)	4.5	0.3
9RN42-B pyrite		400	(2)	2.5	0.3

(1) Isotope ratios were analysed using SIMS.
(2) Isotope ratios were analysed using IRMS.

et al., 2006). This resulted in anhydrite exhibiting similar isotope value as the residual pyrite upon oxidation (Fig. 5). The $\delta^{18}O$ value of anhydrite or aqueous SO_4 formed during oxidation of pyrite will depend on the isotopic value of the source of oxygen in the system namely the surrounding rocks or percolating seawater (Fig. 3) (Seal et al., 2000a).

4.2.4. Volcanic gas-basalt interaction

Interaction of volcanic gas with basalt was simulated to constrain anhydrite formation associated with degassing of magmatic sourced sulfur. Interaction of basaltic rock with condensed volcanic gas containing ~ 2.7 mol% volcanogenic SO_2 led to the formation of small amounts of anhydrite (Fig. 3). Thereby, $\delta^{34}S$ values of anhydrite were predicted to span over a wide range with values of −1.4 to +14‰ at high fluid temperatures (>300 °C) and −1.2 to up to +30‰ at low fluid temperatures (<100 °C) reflecting temperature dependent sulfur isotope fractionation between anhydrite and fluid phase. With progressive reaction, the rock provided a significant source of sulfur for anhydrite leading to an approximation of the $\delta^{34}S$ values of anhydrite to the isotopic value of the basalt. The $\delta^{18}O$ values of the forming anhydrite were found to be dependent

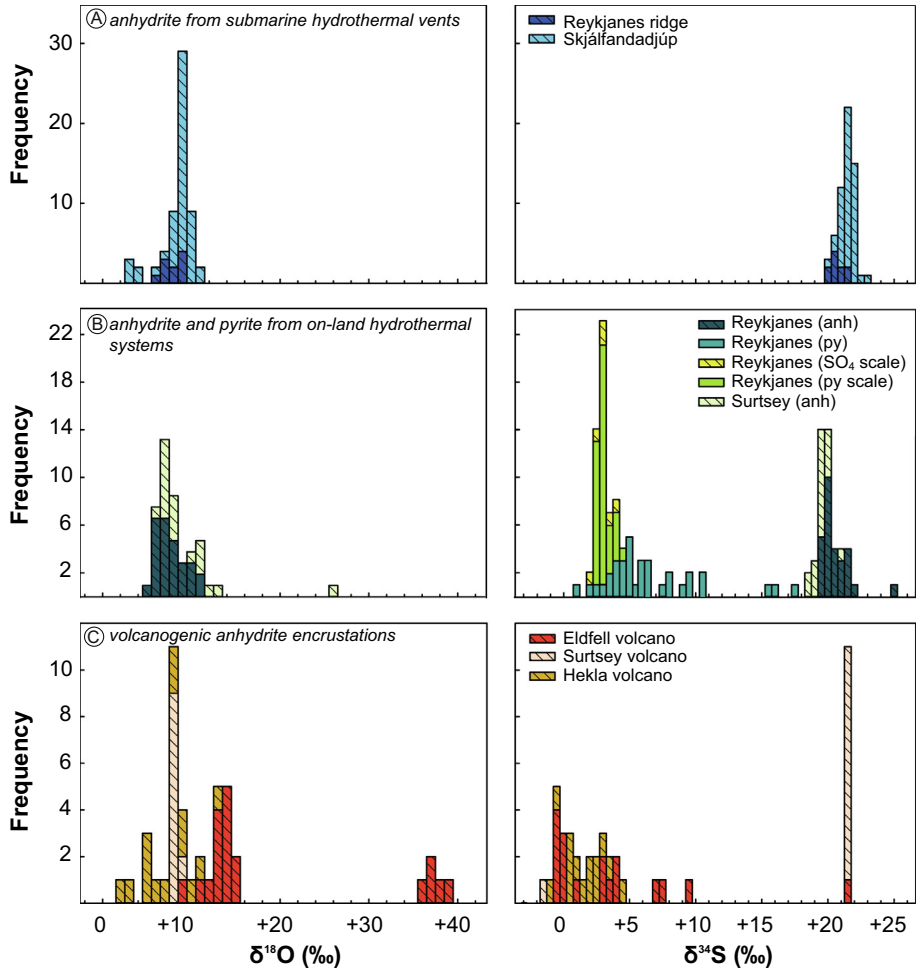

Fig. 2. Distribution of $\delta^{18}O$ and $\delta^{34}S$ in anhydrite (cross-hatched) and pyrite (filled) from (A) submarine hydrothermal vents, (B) on-land seawater-dominated hydrothermal systems, and (C) volcanogenic encrustations. Anh: anhydrite; py: pyrite.

on their formation temperature whereas the extent of basalt reaction had only minor effects on the $\delta^{18}O$ value of anhydrite (Fig. A5).

5. DISCUSSION

5.1. Controls on the isotope composition of anhydrite and pyrite

The measured $\delta^{34}S$ and $\delta^{18}O$ values in anhydrite and pyrite were compared to the results of the geochemical modelling to assess the processes that affect the formation and stable isotope composition of anhydrite and pyrite in MOR related hydrothermal and volcanogenic systems.

Anhydrite from submarine hydrothermal vent systems at Skjálfandadjúp and Reykjanes ridge showed $\delta^{34}S$ values similar to seawater and $\delta^{18}O$ values spreading over a wide range from +2.4 to +10.2‰. The observed isotope variations are best explained by heating of seawater upon conductive heat exchange or heating induced by mixing of seawater with a hydrothermal fluid in proximity of submarine hydrothermal vents without any contribution of seawater-rock interaction processes (Fig. 6). As equilibrium sulfur isotope fractionation between anhydrite and SO_4 is small, $\delta^{34}S$ values in submarine hydrothermal anhydrite reflect the isotope composition of seawater, whereas $\delta^{18}O$ values are mainly dependent on temperature.

In contrast, $\delta^{34}S$ and $\delta^{18}O$ values in anhydrite deriving from on-land seawater-dominated hydrothermal systems at Surtsey and Reykjanes differed from the isotope values of seawater. Such departure from the value of the source fluid is considered to reflect isotopic changes upon progressive basalt alteration associated with heating of seawater (Fig. 6). Upon progressive basalt alteration, the rock becomes an increasingly important source for sulfur and oxygen in anhydrite which implies a shift of the isotope composition towards the isotope value of the rock. A change from fluid to rock dominant source with progressive basalt alteration is not uncommon in hydrothermal systems and has been also reported for the origin of sulfur in hydrothermal anhydrite from the ODP Hole 504B (Alt et al., 1989; Teagle et al., 1998b).

Elevated $\delta^{34}S$ values in hydrothermal pyrite (+3.4 to +19.7‰) from Reykjanes relative to unaltered, undegassed

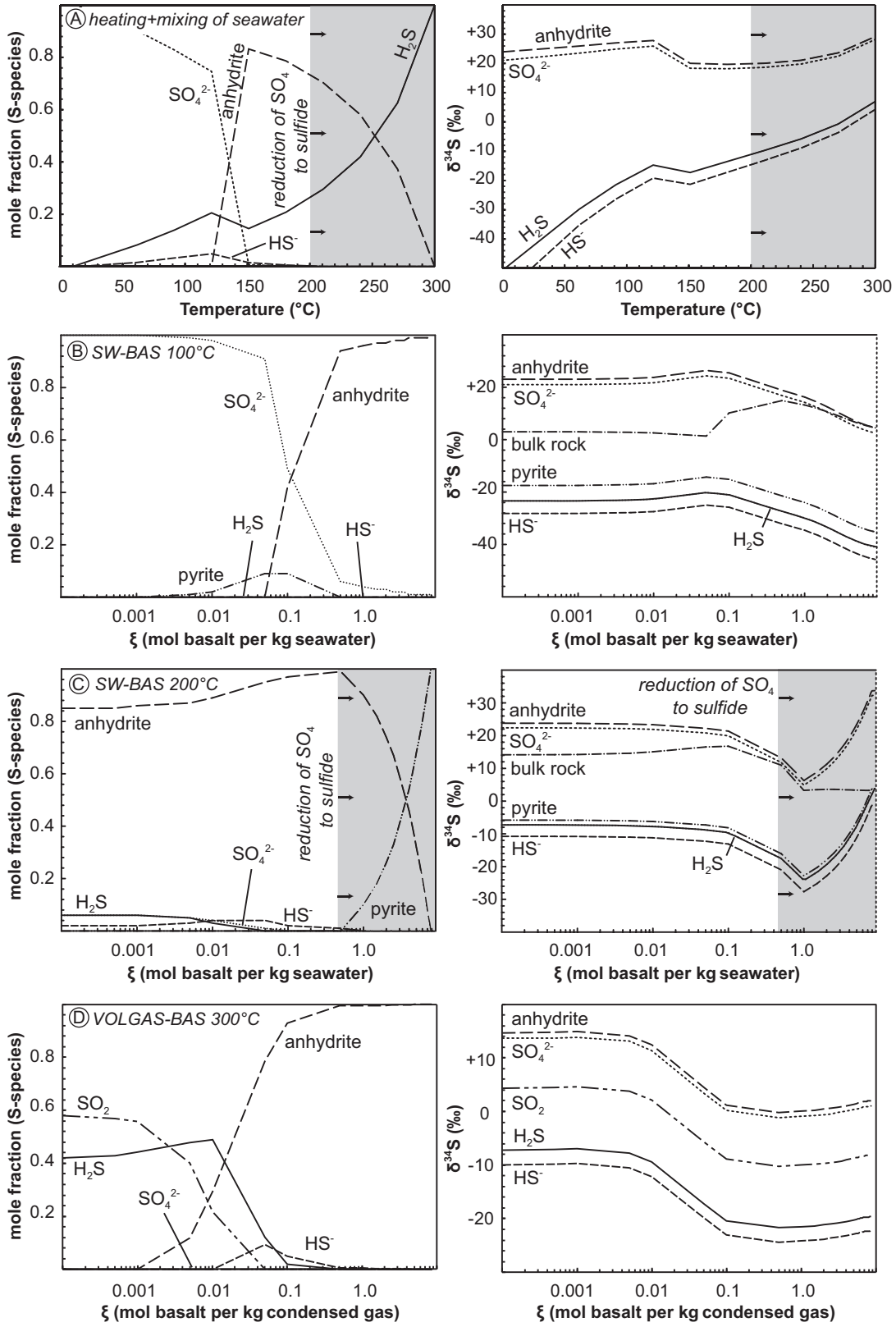

Fig. 3. Modelling results showing the relative abundance of sulfur species in the reacting solution and the sulfur isotope composition of anhydrite, pyrite and aqueous sulfur species as a function of reaction progress ξ (i.e., mol basalt dissolved in 1 kg solution) and temperature for modelling scenarios 1 (A), 2 (B and C) and 4 (D). Details on the modelling calculations are given in Supplement A.

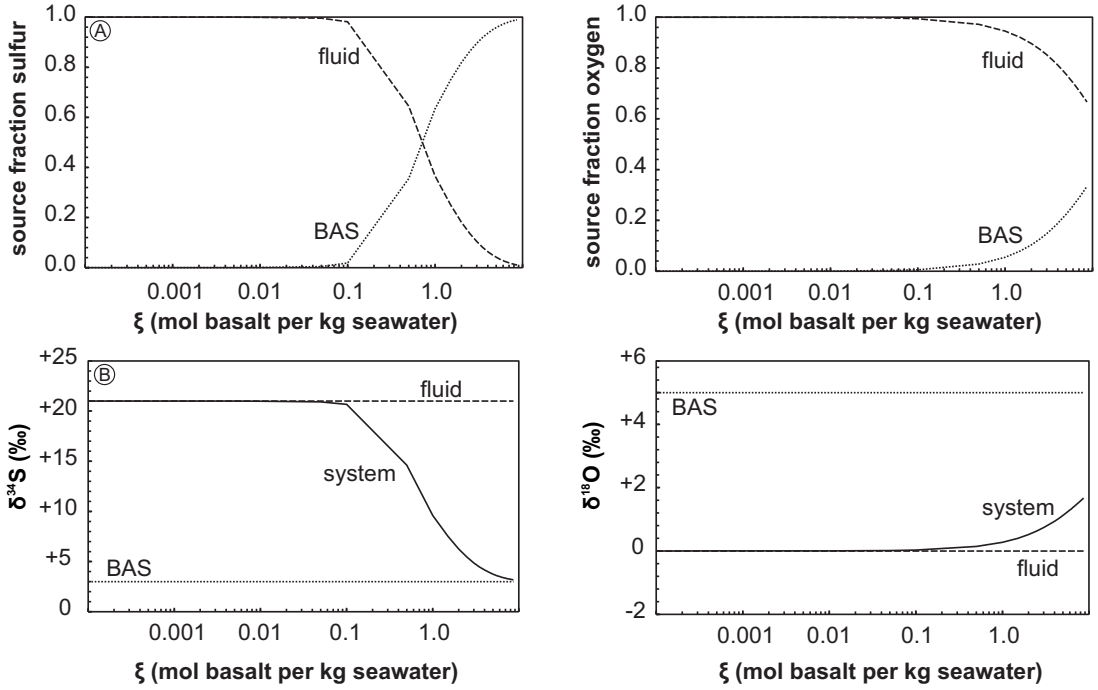

Fig. 4. Results of the source fraction of sulfur and oxygen (A) in the system for the seawater-basalt interaction model. A change in the source from fluid- to rock-dominated occurs upon progressive seawater-basalt interaction. At high reaction progress (i.e., low water–rock ratios), sulfur and oxygen are dominantly provided by the rock. This is also reflected in the change in $\delta^{34}S$ and $\delta^{18}O$ of the system (B) where both $\delta^{34}S$ and $\delta^{18}O$ values approach the isotope value of the rock with progressive reaction. Isotope values for basalt and fluid taken from Halldórsson et al. (2020); Muehlenbachs and Clayton (1976); Tostevin et al. (2014). BAS: basalt.

basalt (−2.5 to 0.0‰; (Halldórsson et al., 2020)) and dissolved sulfide in the geothermal fluid (+0.2 to +5.9‰; (Gunnarsson-Robin et al., 2017)) reflect either input of seawater originated sulfur and/or changes upon basalt alteration and associated reduction of seawater-SO_4 to sulfide (Fig. 5). Upon reduction of seawater-SO_4, the isotopically light molecules are preferentially reduced to sulfide leading to the ^{34}S-enrichment in the residual SO_4 and anhydrite relative to seawater. With progressive reduction, dissolved sulfide and hydrothermal (secondary) pyrite becomes ^{34}S-enriched relative to magmatic (primary) sulfides (Seal, 2006; and references therein). Such ^{34}S-enriched anhydrite and pyrite were found in Reykjanes (this study), ODP Hole 504B and TAG-1 Site 957 indicating that reduction is a likely process occurring within high-temperature (>200 °C) hydrothermal systems (Chiba et al., 1998; Teagle et al., 1998b). The impact of reduction of seawater-SO_4 on the formation of sulfides may have further important implications on the depth of seawater penetration in hydrothermal systems. At Reykjanes, the occurrence of hydrothermal pyrite at > 2000 m depth with a distinct $\delta^{34}S$-seawater signature (+6.8 ± 3.0‰) and permeable feeder zones at depths exceeding 4500 m (Zierenberg et al., 2017) imply that seawater is able to penetrate deep into the hot oceanic crust where seawater-SO_4 may be either removed by anhydrite precipitation and/or quantitative sulfate reduction.

The $\delta^{34}S$ values measured in pyrite (+3.0 ± 0.6‰) and sulfate (+2.9 ± 0.6‰) precipitated in scales within the production pipes of well RN-09 at Reykjanes revealed that sulfur in the hydrothermal fluid discharge mainly derives from remobilization of basaltic sulfur. However, approximately 10–20% of the sulfur in pyrite may derive from seawater-SO_4. Pyrite precipitated in the production pipes due to boiling of the fluid caused by depressurization across flow control orifices (Hardardottir et al., 2010). Upon boiling acid gases partitioned into the steam raising the pH of the fluids causing sulfide saturation and precipitation. Partitioning of dissolved H_2 into the vapor results in oxidation of some dissolved sulfide in the fluid phase to sulfate, which precipitated as anglesite. This rapid oxidation may occur without significant sulfur isotope fractionation between mineral-fluid pairs (Taylor and Wheeler, 1994; Ohmoto and Goldhaber, 1997; Budakoglu and Pratt, 2005; Lefticariu et al., 2006), such that $\delta^{34}S$ of coprecipitated pyrite and sulfate overlap (Fig. 5).

Volcanogenic anhydrite encrustations from Eldfell and Hekla volcano exhibit low $\delta^{34}S$ values (+2.7 ± 3.2‰) with large variations in $\delta^{18}O$ values (+1.4 to +38.0‰) relative to hydrothermal anhydrite. The $\delta^{34}S$ values most likely reflect the isotope composition of the volcanic gas (Fig. 7). As volcanic gases cool < 300–400 °C and condense, SO_2 will disproportionate rapidly into H_2SO_4 and H_2S (Ohmoto and Lasaga, 1982). Further oxidation of H_2S and associated basalt-volcanic gas interaction may eventually lead to SO_4 becoming the dominant sulfur species in the solution and eventually to the formation of anhydrite encrustations. The $\delta^{34}S$ composition of such condensed volcanic gases in Iceland has been reported to range from −1.8 to +3.4‰ (Torssander, 1988). Small equilibrium fractionation

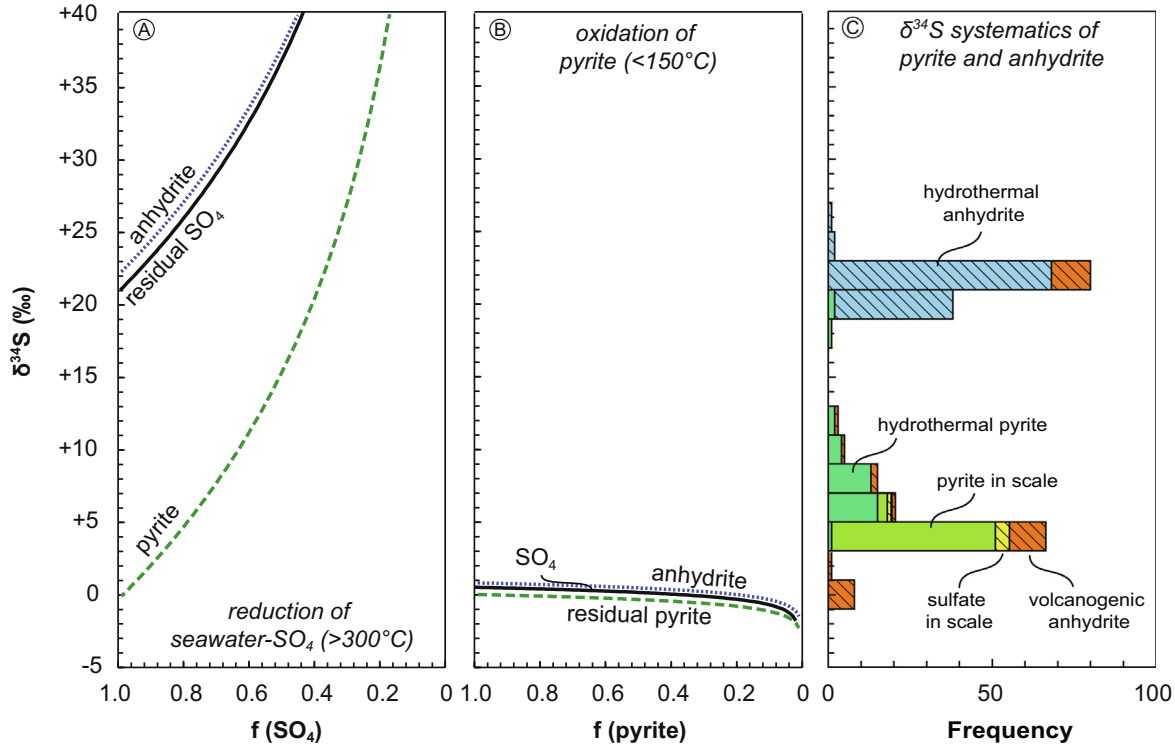

Fig. 5. A Rayleigh model describes $\delta^{34}S$ variations in SO_4, anhydrite and pyrite upon (A) reduction of seawater-SO_4 at elevated temperatures (>300 °C) and (B) oxidation of pyrite at low temperatures (<150 °C). (C) The model trends were compared to $\delta^{34}S$ values measured in hydrothermal anhydrite (Reykjanes ridge, Skjálfandadjúp, Reykjanes) and pyrite (Reykjanes), sulfate and pyrite from scales (Reykjanes) and volcanogenic anhydrite (Eldfell volcano, Surtsey volcano and Hekla volcano). Details on model calculations are given in Supplement A.

between aqueous SO_4 and anhydrite encrustations (Balan et al., 2014; Eldridge et al., 2016), thereby, results in the $\delta^{34}S$ value of the resulting anhydrite is often indistinguishable from the fluid. In contrast, the $\delta^{18}O$ value depends on the source of oxygen namely from the surrounding groundwater and/or from atmospheric O_2 (Seal et al., 2000a). In contrast, volcanogenic anhydrite encrustations from Surtsey volcano exhibit $\delta^{34}S$ and $\delta^{18}O$ values that are similar to seawater which implies that these encrustations most likely formed when hot lava came into contact with seawater during the submarine eruption.

In summary, the observed stable isotope variations in hydrothermal and volcanogenic anhydrite and pyrite depend on a complex interplay between multiple processes such as water–rock interaction, oxidation, and reduction processes. The different processes were incorporated into a comprehensive reaction path model that aims to reproduce the stable isotope compositions in hydrothermal systems at a given temperature range. In the following, we will use the model to quantify the relevant processes and estimate the sulfate budget of the different sulfate reservoirs in the oceanic crust.

5.2. The fate of anhydrite and SO_4 at high hydrothermal temperatures (>200 °C)

In the well-studied seawater-dominated high-temperature hydrothermal system at Reykjanes in Iceland, anhydrite is usually found within the upper 2000 m of the crust where temperatures are below 250 °C (Franzson et al., 2002; Marks et al., 2011; Padilla et al., 2012; Zierenberg et al., 2017). In contrast, the oceanic crust, remains a highly under sampled system, where only Holes 504B and 1256D penetrate intact oceanic crust to the gabbroic layer. Thus, to date, there is only little evidence that anhydrite occurs within the dike and gabbroic sections where temperatures may exceed 250 °C (Bruland, 1983; Kusakabe et al., 1989; Alt and Anderson, 1991; Ólafsson et al., 1991; Teagle et al., 1998b, c; Alt et al., 2010; Alt and Shanks, 2011; Stefánsson et al., 2017a; Kelemen et al., 2020a; Kelemen et al., 2020b). In hydrothermal fluids exhibiting temperatures above 250 °C discharged from axial regions, SO_4 is almost absent and total sulfur concentrations (4.4–8.8 mmol kg^{-1}) are significantly lower than those of seawater (Lilley et al., 2003; Ono et al., 2007; Stefánsson et al., 2015). The absence of SO_4 in these fluids has been previously explained by reduction of seawater-SO_4 to H_2S, pyrite formation (Shanks III et al., 1981; McDuff and Edmond, 1982) and/or anhydrite deposition upon temperature increase or fluid mixing of cool recharge with hot discharge fluids (Seyfried Jr and Bischoff, 1979; Teagle et al., 1998b; Barker et al., 2010).

Our geochemical isotope model revealed, that at > 200 °C, quantitative anhydrite formation limits the SO_4 fluid concentration. Gunnarsson-Robin et al. (2017) demonstrated that in seawater-dominated high-

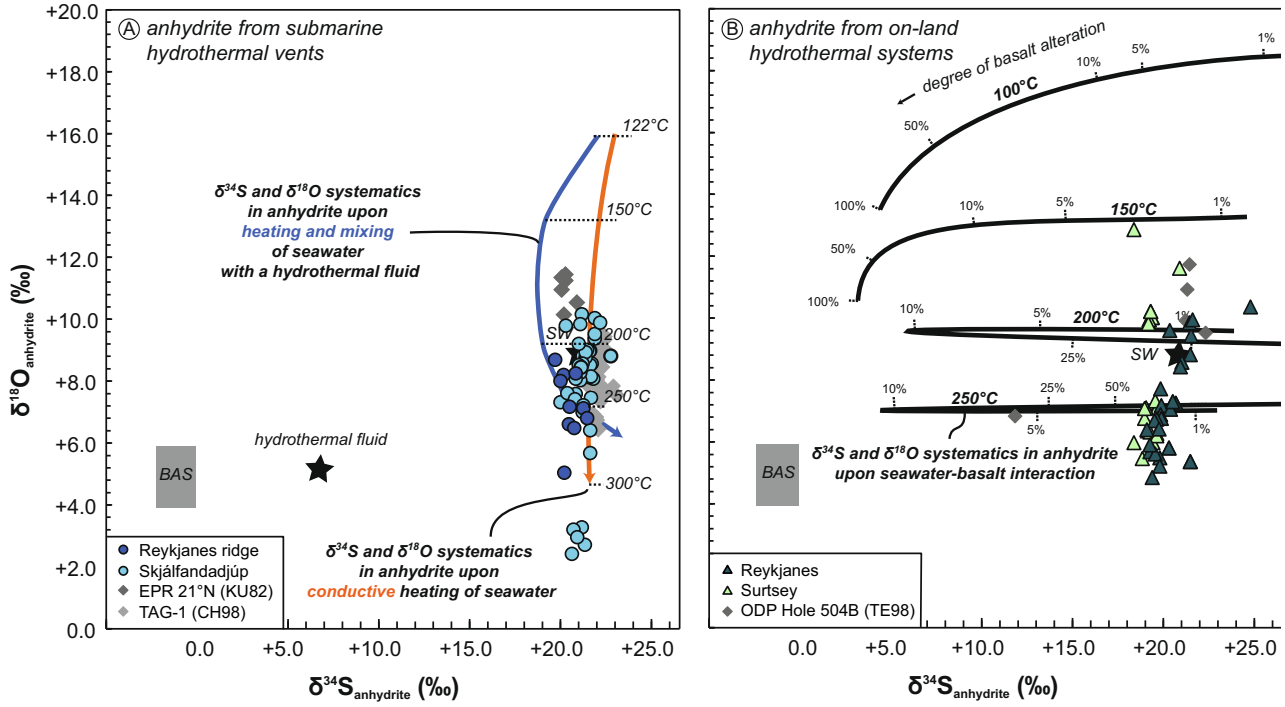

Fig. 6. Comparison of reaction paths from geochemical isotope modelling with natural $\delta^{18}O$ and $\delta^{34}S$ systematics of anhydrite from (A) submarine hydrothermal vents at Reykjanes ridge and Skjálfandadjúp and (B) on-land seawater-dominated hydrothermal systems at Reykjanes and Surtsey. Solid lines indicate the modeled $\delta^{18}O$ and $\delta^{34}S$ systematics in anhydrite upon conductive heating of seawater (red arrow), heating and mixing of seawater with a hydrothermal fluid (blue arrow) and progressive seawater-basalt interaction (black lines) at various temperatures. Also shown are $\delta^{18}O$ and $\delta^{34}S$ values previously reported from the ODP Hole 504B, East Pacific Rise (EPR) and the Trans-Atlantic Geotraverse (TAG-1). Input parameters in our modelling scenarios are given in the supplementary material. The chemical and isotope composition of the hydrothermal fluid was taken from (Von Damm et al., 1985b; Von Damm, 1990; McDermott et al., 2015). BAS: basalt (Muehlenbachs and Clayton, 1976; Halldórsson et al., 2020); SW: seawater-SO_4 (Kusakabe et al., 1982; Tostevin et al., 2014); TE98: Teagle et al. (1998b); KU82: Kusakabe et al. (1982); CH98: Chiba et al. (1998).

temperature hydrothermal systems, almost 99% of fluid SO_4 may be sequestered into anhydrite prior to reduction of the residual SO_4 to sulfide to explain observed sulfur concentrations and $\delta^{34}S$ values of hydrothermal fluid discharge at Reykjanes. Consequently, sulfur concentrations in the reducing solution might be significantly lower than those of the initially oxidized source fluid. This implies that the contribution of seawater sourced sulfur is rather small in hydrothermal vent systems along MORs where fluid discharge is considered to be reduced (e.g., Lilley et al., 2003; McDermott et al., 2015; Ono et al., 2007; Von Damm et al., 1985a; Von Damm, 1995; Von Damm et al., 1995). In fact, the $\delta^{34}S$ values reported for discharge of MOR-related hydrothermal vents are ^{34}S-depleted (+1 to +7‰) relative to seawater (McDermott et al., 2015).

Recently reported $\delta^{34}S$ data on high-temperature (264–292 °C) hydrothermal reservoir fluids from Reykjanes showed that the SO_4 in the seawater-dominated hydrothermal system had high $\delta^{34}S$ values (+21.1 to +24.1‰) indicating a seawater source, whereas $\delta^{34}S$ of S^{-II} indicated values (-0.4 to +5.8‰) dominated by dissolution of basaltic sulfide and H_2S degassing from melt with only a small (0–25%) contribution from reduced seawater-SO_4 (Gunnarsson-Robin et al., 2017). This is in line with our findings which showed that a finite amount of seawater-SO_4 will persist in the hydrothermal fluid in equilibrium with anhydrite (~0.3 to 6.2 μmol kg^{-1}; Table A7) at > 200 °C. This implies that sulfur emitted from hydrothermal vents along MORs may likely be of dominantly magmatic origin either from direct degassing of H_2S or leaching of sulfur from the quenched rocks rather than deriving from recycled and reacted seawater. In fact, hydrothermal dissolution of igneous sulfur from sheeted dikes and hydrothermally altered gabbro together with loss of SO_4 as anhydrite followed by sulfate reduction has been shown to produce fluids containing sulfide concentrations similar to hydrothermal vents (Alt, 1994, 1995; Alt and Shanks III, 2003).

5.3. The fate of anhydrite and SO_4 at low hydrothermal temperatures (<150 °C)

Large quantities of anhydrite have been predicted to occur in the oceanic crust upon infiltration and heating of seawater in vicinity of MORs (Seyfried Jr and Bischoff, 1979; Teagle et al., 1998b; Barker et al., 2010; Gunnarsson-Robin et al., 2017). However, to date, ODP/DSDP drilling projects have only recovered relatively small amounts of anhydrite from the upper oceanic crust (Alt, 2003; Teagle et al., 2006; Alt et al., 2010). The reasons for

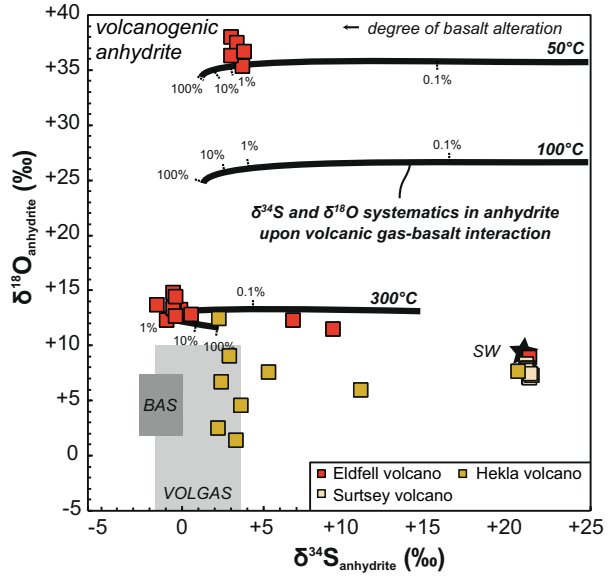

Fig. 7. Comparison of reaction paths from geochemical isotope modelling with natural $\delta^{18}O$ and $\delta^{34}S$ systematics of anhydrite from volcanogenic incrustations at Eldfell, Surtsey and Hekla volcano. Black lines indicate the modeled $\delta^{18}O$ and $\delta^{34}S$ systematics in anhydrite upon progressive volcanic gas-basalt interaction and heating of seawater at various temperatures. Input parameters in our modelling scenarios are given in the supplementary material. BAS: basalt (Halldórsson et al., 2020); SW: seawater SO_4 (Kusakabe et al., 1982; Tostevin et al., 2014); VOLGAS: volcanic gas (Torssander, 1988).

that are manyfold and may include the lack of appropriate samples from the sheeted dikes and volcanic sections, low core recoveries and thus possible loss of fragile anhydrite veins, retrograde dissolution of anhydrite upon cooling and/ or diffuse leaking of SO_4-bearing fluids from axial systems (Sleep, 1991; Teagle et al., 1998b; Lowell et al., 2003; Teagle et al., 2003; Teagle et al., 2006; Barker et al., 2008; Harris et al., 2017). Anhydrite relicts were found to be preserved in the sheeted dike section of the 11.5 Ma old Macquarie Island ophiolite and within the layered gabbro section in the 95 Ma old Samail ophiolite in Oman (Alt et al., 2003; Kelemen et al., 2020a; Kelemen et al., 2020b). Anhydrite in shallower sections of the ophiolites, however, are rarely preserved (Martin et al., 2021). This could imply that anhydrite might have been locally preserved in old crust at elevated temperatures whereas at lower temperatures retrograde dissolution or hydration of anhydrite to gypsum by meteoric water infiltration during uplift may cause the disappearance of anhydrite (Martin et al., 2021).

To simulate the fate of anhydrite upon cooling of a hydrothermal system within the oceanic crust, we expanded our isotope geochemical modelling following a similar approach as recently introduced for the assessment of water contents in the altered oceanic crust (Kleine et al., 2020a). In brief, mineral modes and $\delta^{34}S$ values of anhydrite were calculated for varying degrees of alteration of the oceanic crust along simplified geotherms representing young (<10 Ma) and old (<100 Ma) oceanic crust, respectively (Table A8, Fig. 8). To verify our modelling approach, we

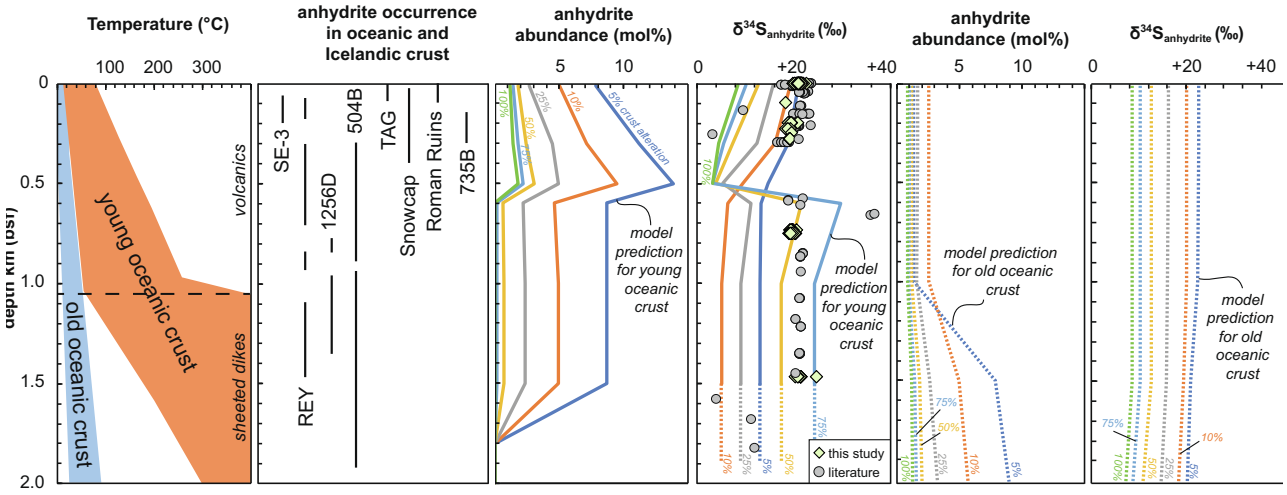

Fig. 8. Abundance and $\delta^{34}S$ of anhydrite calculated along typical geotherms of the young (<10 Ma) and old (>100 Ma) oceanic crust (Nehlig and Juteau, 1988; Alt et al., 1996; Gillis et al., 2001; Wheat and Mottl, 2004; Heft et al., 2008; Alt et al., 2010; Edwards et al., 2012; Grose and Afonso, 2013) for various degrees of alteration (coloured lines). The modelled predictions were compared with natural occurrence and $\delta^{34}S$ of anhydrite reported from DSDP/ODP drill holes into the relatively young (<15 Ma) oceanic and Icelandic crust (this study; Alt and Anderson, 1991; Alt et al., 2010; Alt and Shanks, 2011; Chiba et al., 1998; Craddock and Bach, 2010; Kusakabe et al., 1989; Peters et al., 2010; Teagle et al., 1998a; Teagle et al., 1998b). Measured isotope values of anhydrite in the dike section correspond to a model scenario where the oceanic crust has been altered significantly (illustrated by the yellow and bright blue line) whereas within the volcanics, isotope values of anhydrite indicate that crust alteration has not proceeded far (illustrated by the orange and dark blue line). This information can then be used to decipher the approximate abundance of anhydrite in the respective sections of the crust. The estimates on the degree of alteration of the crust should be treated with caution. It is not implied that the oceanic crust has been altered at 50–75% in the dike section. As alteration at this depth is often non-pervasive (Honnorez et al., 1983; Alt et al., 1996; Teagle et al., 1996) the modelled alteration values are restricted to more altered sections along veins and faults where easy access of seawater is guaranteed. Note that no data is yet available for crust > 15 Ma, thus our model predictions for old oceanic crust can be only viewed as a possible prediction.

Table 3
The S flux estimates to and from each sulfate reservoir in the oceanic crust. Details and input parameters for the calculations are given in Supplement A.

	This study	Alt (2003)	Teagle et al. (1998b)	Alt (1995)	Wheat and Mottl (2000), von Damm (2000) [a]	von Damm (1995) [a]	Gunnarsson et al. (2017) [a]	Kelley et al. (2001) [a]	Mottl (1989), Wheat and Mottl (2000) [a]	Mottl (1989), Wheat and Mottl (2000) [a]	Wheat et al. (2017) [a]	Kleine et al. (2020)
Method	Based on fluid data from geochemical model	Based on fluid data from Elderfield and Schultz (1996) and references therein	Based on S budget of veins and whole rock from Hole 504B	Based on S budget of composites from Holes 504B and 735B	Based on fluid data from EPR	Based on fluid data from Endeavour	Based on fluid data from Reykjanes	Based on fluid data from Lost City	Based on fluid data from Baby Bare	Based on fluid data from the Costa Rica rift flank	Based on fluid data from Dorado seamount	Based on fluid data from Surtsey
Geological setting		Ridge/MOR	Ridge/young oceanic crust	Ridge/young oceanic crust	Ridge/MOR	Ridge/MOR	Ridge/young Icelandic crust	Ridge-flank/young oceanic crust	Ridge-flank/young oceanic crust	Ridge-flank/young oceanic crust	Ridge-flank/young oceanic crust	Ridge-flank/young Icelandic crust
Discharge temperature (°C)	10–300				>300	>300	200–230	50	25–63	58	10	44–138
SO_4 concentration (mmol kg^{-1})	See Table A8	0–0.6			9.0–17.0	2	0.3–1.5	5.0–12.9	17.8	17.0	27.8	10.8–19.4
Fluid mass flux (kg yr^{-1})	$3.1–4.2 \times 10^{13}$ (MOR) [b], 0.1–11×10^{15} (Ridge-flanks, old oceanic crust) [c]	3.7×10^{13}	$1.7–3.5 \times 10^{13}$		$3.1–4.2 \times 10^{13}$ [b]	3.1–4.2×10^{13} [b]	3.1–4.2×10^{13} [b]	0.9–11×10^{15} [c]	0.9–11×10^{15} [c]	0.9–11 $\times 10^{15}$ [c]	0.9–11 $\times 10^{15}$ [c]	0.1–1.2×10^{15}
Seawater-SO_4 flux (Tg yr^{-1}) into the oceanic crust in vicinity of MORs												
	27–38	25	15–31		11–26	26–35	27–37					
SO_4 uptake (Tg yr^{-1}) upon anhydrite formation in vicinity of MORs												
	15–38 (<200 °C) 3–38 (>200 °C)		~2	0.15								
SO_4 flux (Tg yr^{-1}) being reduced to sulfide												
	0.1–30											
Seawater-SO_4 flux (Tg yr^{-1}) to MOR-related hydrothermal vents												
	0.1–3.4											
SO_4 flux (Tg yr^{-1}) from MOR-related high-temperature (>200 °C) hydrothermal vents												
					9–12	2–3	1.0–1.5					
SO_4 flux (Tg yr^{-1}) returning to the ocean (e.g., upon retrograde dissolution of anhydrite, leakage of SO_4-bearing fluids from the crust)												
	0.3–4 (10% loss of anhydrite) 2–23 (60% loss of anhydrite)		11–27									
SO_4 uptake (Tg yr^{-1}) upon low-temperature seafloor alteration (e.g., anhydrite formation, oxidation of SO_4 to pyrite upon microbial processes)												
								17–55	10–49	10–22	2–5	0.9–29

[a] fluxes in this table were calculated from the SO4 concentrations reported for the respective sites and the hydrothermal fluid flux given in this table.
[b] fluid mass flux taken from Mottl (2003).
[c] fluid mass flux calculated using Eq. (A14) after Elderfield and Schultz (1996).

compared the modelling results with previously reported abundances and isotope compositions of anhydrite retrieved from the altered oceanic crust (Kusakabe et al., 1989; Alt and Anderson, 1991; Chiba et al., 1998; Teagle et al., 1998a; Teagle et al., 1998b; Alt et al., 2010; Craddock and Bach, 2010; Peters et al., 2010; Alt and Shanks, 2011).

Our model predicted that anhydrite is most abundant within the upper 1000 m of young oceanic crust (Fig. 8) where $\delta^{34}S$ of anhydrite is mainly controlled by the isotopic composition of the infiltrating seawater (Teagle et al., 1998b). Anhydrite formation will be induced by progressive seawater-rock interaction and heating the infiltrating seawater either conductively or by mixing with a hot hydrothermal fluid (e.g., Skikazono et al., 1983; Teagle et al., 1998a; Teagle et al., 1998b; Teagle et al., 1998c; Lowell et al., 2003; Kawada and Yoshida, 2010). At shallow depth and relatively low temperatures (<10 °C), $\delta^{18}O$ in anhydrite and dissolved SO_4 may be affected by sluggish exchange of sulfate-oxygen-fluid exchange causing disequilibrium between dissolved sulfate and seawater (Chiba et al., 1981; Chiba and Sakai, 1985). With increasing depth (>1000 m), seawater-basalt ratios ultimately decrease due to limits in fluid accessibility and $\delta^{34}S$ values of anhydrite are consequently mainly controlled by the isotopic composition of the host rock and/or redox processes. At these depths or temperatures of > 200 °C, reduction of SO_4 to sulfide becomes a significant process limiting the abundance of anhydrite at greater depths (Fig. 8).

Our geochemical model suggests that upon progressive cooling of the crust, anhydrite formation within the upper 1500 m is limited due to retrograde solubility and/ or colder temperatures (Fig. 8). Retrograde solubility of anhydrite upon cooling of the uppermost (<1000 m) oceanic crust may thus play a critical role in recycling of formerly sequestered SO_4 to the oceans. The $\delta^{34}S$ values of such anhydrite relicts are predicted to be either similar to the corresponding seawater isotopic value or slightly less positive. As equilibrium isotope fractionation factors between anhydrite and seawater lay within +2.5‰ at < 50 °C (Balan et al., 2014; Eldridge et al., 2016), dissolution and recycling of SO_4 deriving from anhydrite would not greatly affect the isotopic composition of the pore fluid and residual anhydrite. Limited anhydrite formation is also reflected in discharge fluid chemistries from ridge flank hydrothermal systems where SO_4 concentrations are slightly lower and/or similar to the respective concentrations of seawater (Mottl, 1989; Mottl and Wheat, 1994; Wheat et al., 1996; Mottl et al., 1998; Wheat and Mottl, 2000; Wheat and Fisher, 2008; Coogan et al., 2019; Wheat et al., 2019). Deviations in SO_4 concentrations from seawater in these settings were attributed to reduction of seawater-SO_4 and formation of sulfides through microbial processes inferring that uptake of SO_4 by anhydrite formation is rather unlikely within colder regimes of the oceanic crust (Wheat and Mottl, 2000; Wheat and Fisher, 2008; Alford et al., 2011; Alt and Shanks, 2011; Lever et al., 2013). However, in the seawater-dominated low-temperature hydrothermal system at Surtsey, the observed decrease in SO_4 concentrations of borehole fluids relative to seawater was explained by anhydrite formation (Jakobsson and Moore, 1986; Kleine et al., 2020b). At depths > 1000 m in old oceanic crust, our model predicts that temperatures may remain sufficiently high to preserve anhydrite. To date, no hole has reached the sheeted dike section or deeper depths of old oceanic crust to verify the model predictions. However, the occurrence of anhydrite relicts in the Macquarie Island and Samail ophiolite may point towards an increased likelihood that anhydrite may be preserved deep within the aging oceanic crust (Alt et al., 2003; Kelemen et al., 2020a; Kelemen et al., 2020b).

5.4. Sulfate recycling in the igneous oceanic crust

The SO_4 flux into the crust in vicinity of MORs has been well established over the past decades (Staudigel, 2014; and references therein). However, to date, there are only a few flux estimates available that constrain the amount of SO_4 that might be regained to the oceans via axial regions or through retrograde dissolution of anhydrite upon cooling of the oceanic crust (Sleep, 1991; Teagle et al., 1998b). Our geochemical isotope modelling approach simulates the stable isotope variations of anhydrite upon water–rock interaction and associated reduction and oxidation processes. Moreover, it delivers estimates and predictions on the modal abundance of anhydrite, sulfide and SO_4 concentrations of the reacting solution and source fraction of sulfur in the system. These parameters together with estimates of the fluid mass flux were combined into a mass balance model to constrain the chemical fluxes from and to each SO_4 reservoir in the oceanic crust (Fig. 9, Table 3). Details on the flux calculations and input parameters are given in the supplementary material.

Chemical fluxes can be obtained from elemental concentrations of discharge fluids and hydrothermal fluid mass flux that circulates through the oceanic crust. The hydrothermal fluid mass flux can be calculated using heat flux, heat capacity of seawater, and the change in water temperature from bottom of the ocean to aquifer temperatures (Kadko et al., 1995; Elderfield and Schultz, 1996; Mottl, 2003), or geochemical and/or isotopic tracers such as thallium, lithium, sulfur, or strontium (Palmer and Edmond, 1989; Bickle and Teagle, 1992; Teagle et al., 1998b; Chan et al., 2002; Nielsen et al., 2006; Barker et al., 2010; Harris et al., 2017). Discrepancies in the hydrothermal fluid flux estimates have been discussed previously in the literature and are often dependent on the approach used for their determination (e.g., Alt, 2003; Harris et al., 2017). For the axial regions, alteration, Sr, and S budgets of the oceanic crust suggest that the hydrothermal fluid flux might be relatively small or 0.5–3. 5×10^{13} kg yr^{-1} (Teagle et al., 1998b; Harris et al., 2017) whereas flux estimates based on the Sr budget of seawater were estimated to be one magnitude larger (Palmer and Edmond, 1989). Here, we use a hydrothermal flux of 3.70 $\pm$ 0.51 $\times$ 10^{13} kg yr^{-1} (Mottl, 2003) for chemical flux estimates in the axial regions which has been established as one of the most robust flux values for the MOR system (Alt, 2003). Mottl (2003) based the hydrothermal flux on the available energy to hot hydrothermal fluids, from the cool-

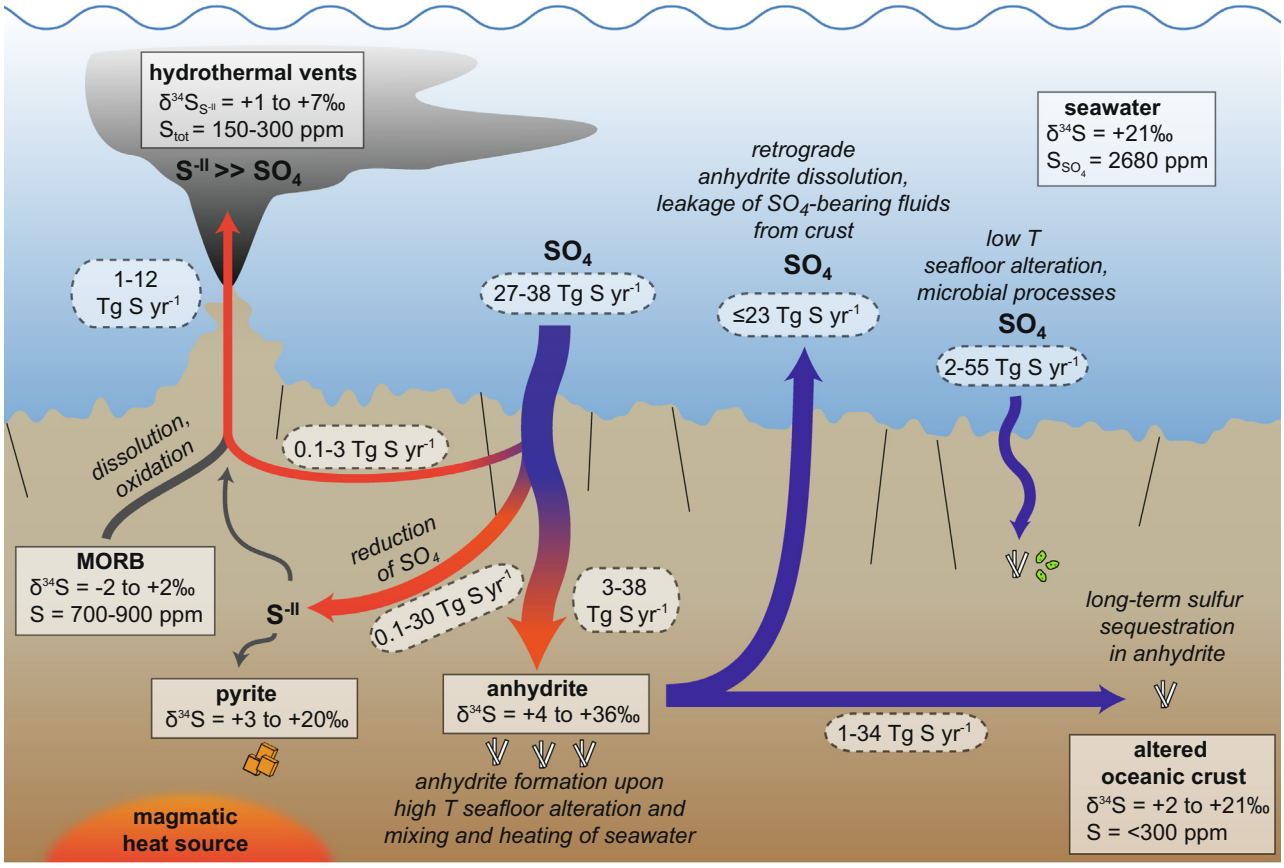

Fig. 9. The SO_4 flux estimates (in Tg S yr^{-1}) for the sulfate reservoirs in the oceanic crust (see also Table 3; flux estimates in the figure are rounded). Details on the flux calculations can be found in Supplement A. Flux estimates for anhydrite formation upon low-temperature seafloor alteration were taken from Mottl (1989); Wheat and Fisher (2008); Wheat and Mottl (2000). Sulfur isotope values for seawater, altered oceanic crust, MORB and hydrothermal vents are taken from Bruland (1983); Lilley et al. (2003); McDermott et al. (2015); Ono et al. (2007); Saal et al. (2002); Torssander (1988, 1989); Von Damm (2000). Sulfur isotope values for anhydrite and pyrite are taken from this study; Alt and Anderson (1991); Alt et al. (2010); Alt and Shanks (2011); Chiba et al. (1998); Craddock and Bach (2010); Kusakabe et al. (1989); Peters et al. (2010); Teagle et al. (1998a); Teagle et al. (1998b).

ing and crystallization of magma forming new crust at mid-ocean ridges. For estimating the chemical flux through ridge-flanks and old oceanic crust we use hydrothermal fluid fluxes that are based on the approach presented by Elderfield and Schultz (1996) (see supplementary material for calculation details) which seems to deliver reasonably realistic flux estimates for off-rift regions of the oceanic crust (Coogan and Gillis, 2018 and references therein).

Based on our flux calculations and modelling results, the major uptake (3–38 Tg S yr^{-1}) of seawater-SO_4 by anhydrite formation occurs upon heating of seawater through mixing with hydrothermal fluids and associated seawater-basalt interaction in vicinity of MORs (Fig. 9). Reported estimates on the SO_4 uptake by anhydrite based on rock records yielded 0.15–2 kg S yr^{-1} (Alt, 1995a; Teagle et al., 1998b). Alt, (1995) and Teagle et al., (1998b) obtained their flux values from the sulfur budget of composites and cores recovered from Holes 504B and 735B. However, this rock-based chemical flux estimate might suffer from low core recoveries and thus might represent a lower limit of the annual S uptake of the crust by anhydrite formation. Although, reduction processes may limit the formation of anhydrite at elevated temperatures (>200 °C), most anhydrite formation is expected to occur within colder (50–150 °C) regions of MOR-related hydrothermal systems (Fig. 8). The sulfur storage capacity of anhydrite, however, will most likely decrease with cooling and aging of the crust due to retrograde solubility of anhydrite (Sleep, 1991). Our model predicts that up to 60% of the formerly sequestered sulfate may return to the oceans upon retrograde dissolution of anhydrite which results in a flux of up to 22.8 Tg S yr^{-1} recycled to the oceans each year. In comparison, Teagle et al. (1998b) estimated a flux of 11–42 Tg S yr^{-1} returning to the oceans through leaking of SO_4-bearing fluids from the crust. The amount of SO_4 sequestered long-term in anhydrite was estimated to range from 1.2 to 34 Tg S yr^{-1}. Seawater-SO_4 may also (re-) enter the oceanic crust through hydrothermal systems in the ridge flanks or seamount conduits (Mottl, 1989; Wheat and Mottl, 2000; Wheat and Fisher, 2008). Based on reported SO_4 concentrations and hydrothermal fluid mass fluxes of ridge flank systems we estimate this flux to

be 0.9–49 Tg S yr^{-1}. Low SO_4 concentrations relative to seawater in these systems were explained by either reduction of SO_4 to pyrite through microbial processes (Mottl, 1989; Wheat and Mottl, 2000; Wheat and Fisher, 2008) or anhydrite formation (Jakobsson and Moore, 1986; Kleine et al., 2020b).

Furthermore, we can use our modelling approach to estimate the contribution of seawater-SO_4 to sulfate emissions at MORs. The amount of seawater-derived SO_4 emitted at high-temperature MOR-related hydrothermal systems (0.1–3.0 Tg S yr^{-1}) is rather small relative to the total SO_4 flux (1–12 g S yr^{-1}) in vent discharges calculated from measured SO_4 concentrations (1.0–9.0 mmol kg^{-1}) in the high-temperature hydrothermal vent systems at the EPR and Endeavour (Von Damm, 1995, 2000) and the seawater-dominated hydrothermal system at Reykjanes (Gunnarsson-Robin et al., 2017). Sulfate emitted from high-temperature hydrothermal vents may dominantly derive from leaching and oxidation of primary basalt and sulfides. The contribution of seawater-derived SO_4 is limited due to effective reduction of SO_4 to S^{-II} and subsequent pyrite formation at elevated temperatures.

Note, that calculated flux estimates in this study are highly dependent on estimates given for the hydrothermal fluid mass flux circulating through axial and ridge flank regions of the oceanic crust. Here, our chemical flux estimates agree reasonably well with previously reported flux values. Our model can be easily adjusted to future findings on hydrothermal fluid fluxes in axial and non-axial regions or insights on the whereabouts of anhydrite in the oceanic crust. In particular the low-temperature sulfate cycle remains a subject of debate. Too little is known about the abundance of anhydrite in old (>100 Ma) igneous oceanic crust. However, we show that leaching of primary sulfur from mid-ocean ridge basalt (MORB) as well as removal of anhydrite upon cooling and aging of the oceanic crust will ultimately decrease the sulfur content of altered igneous oceanic crust which agrees well with previous findings on low sulfur concentrations in subduction related volcanics and slab-derived metabasalts (Ishihara and Sasaki, 1989; Bernard et al., 1996; Imai et al., 1996; De Hoog et al., 2001; Luhr, 2008; Li et al., 2020). This demonstrates that our model may provide a valuable tool to constrain sulfate fluxes for the various sulfate reservoirs within the oceanic crust.

6. CONCLUSIONS

In this study, the stable isotope composition ($\delta^{34}S$, $\delta^{18}O$) of anhydrite and pyrite collected along the submarine and on-land section of the MAR were utilized to investigate the key variables (e.g., extent of fluid-rock reaction, temperature, redox conditions, source of reacting fluids and rocks) that control anhydrite formation and sulfate recycling in the crust. The $\delta^{34}S$ values of hydrothermal anhydrite clustered at $+20.6 \pm 1.0‰$ whereas volcanogenic anhydrite in encrustations were significantly ^{34}S-depleted. Hydrothermal pyrite exhibited $\delta^{34}S$ values ranging from +3.4 to +19.7‰. The $\delta^{18}O$ were found to vary strongly depending on the formation temperature of anhydrite. Geochemical isotope modelling revealed that the isotope composition of anhydrite and pyrite is controlled by the source of elements (fluid or rock). With progressive alteration (or extent of reaction), both sulfur and oxygen in anhydrite may derive from the host rock resulting in $\delta^{34}S$ and $\delta^{18}O$ values of anhydrite approaching host rock isotope values. At elevated temperatures, reduction of SO_4 to sulfide results in the increase of $\delta^{34}S$ of the residual sulfate and consequently rather positive $\delta^{34}S$ values in precipitating anhydrite relative to non-reduced seawater-SO_4.

Our geochemical isotope modelling approach further provides a useful tool to predict and simulate the systematics of modal abundance of anhydrite as a function of depth and temperature upon basalt alteration in the oceanic crust. This allows estimation of the SO_4 fluxes to and from the major sulfate reservoirs in the oceanic crust. Anhydrite plays a key role in sequestering seawater-SO_4 along MORs. However, sequestration of sulfur in anhydrite is not long-lasting as SO_4 liberated due to retrograde solubility of anhydrite returns to the seawater cycle with an only slightly modified isotope composition. The removal of anhydrite upon cooling and aging of the crust could ultimately result in a loss of up to 60% of the sulfur originally accumulated upon hydrothermal alteration in vicinity of mid-ocean ridges.

Declaration of Competing Interest

The authors declare that they have no known competing financial interests or personal relationships that could have appeared to influence the work reported in this paper.

ACKNOWLEDGEMENT

This project was financially supported by the University of Iceland Recruitment fund, the. International Continental Scientific Drilling Program (ICDP) through a grant to the SUSTAIN project, the Icelandic Science Fund, ICF-RANNÍS (project number: 163083-051), the Bergen Research Foundation and K.G. Jebsen Centre for Deep Sea Research at University of Bergen, Norway, the German Research Foundation (DFG), and DiSTAR, Federico II, University of Naples, Federico II, Italy. The University of Utah, USA and the two Icelandic power companies Reykjavík Energy and Landsvirkjun, contributed additional funds. HS Orka kindly provided access to the drill cuttings and core at Reykjanes. G.H. Gudfinnsson, H. Jeon and K. Lindén are thanked for assistance during sample preparation and data acquisition. We would like to thank J. G. Catalano and D.A.H. Teagle for careful editorial handling and three anonymous reviewers for their constructive reviews which significantly improved this study. This is NordSIMS contribution #692.

APPENDIX A. SUPPLEMENTARY DATA

Supplementary data to this article can be found online at https://doi.org/10.1016/j.gca.2021.10.016.

REFERENCES

Alford S. E., Alt J. C. and Shanks, III, W. C. (2011) Sulfur geochemistry and microbial sulfate reduction during low-temperature alteration of uplifted lower oceanic crust: Insights from ODP Hole 735B. *Chem. Geol.* **286**, 185–195.

Alt-Epping, P. and Diamond, L.W. (2008) Reactive transport and numerical modeling of seafloor hydrothermal systems: a review. Modeling Hydrothermal Processes at Oceanic Spreading Centers: Magma to Microbe. AGU Monograph, Washington, DC, 167–192.

Alt J. C. (1994) A sulfur isotopic profile through the Troodos ophiolite, Cyprus: primary composition and the effects of seawater hydrothermal alteration. *Geochim. Cosmochim. Acta* **58**, 1825–1840.

Alt J. C. (1995) Sulfur isotopic profile through the oceanic crust: Sulfur mobility and seawater-crustal sulfur exchange during hydrothermal alteration. *Geology* **23**, 585–588.

Alt J. C. (1995b) Subseafloor processes in mid-ocean ridge hydrothermal systems. In *Seafloor Hydrothermal Systems: Physical, Chemical, Biological, and Geological Interactions* (eds. S. E. Humphris, R. A. Zierenberg, L. S. Mullineaux and R. E. Thomson). Geophysical Monograph Series, pp. 85–114.

Alt J. C. (2003) Hydrothermal fluxes at mid-ocean ridges and on ridge flanks. *Comptes Rendus Geosci.* **335**, 853–864.

Alt J. C. and Anderson T. F. (1991) Mineralogy and isotopic composition of sulfur in layer 3 gabbros from the Indian Ocean, Hole 735B. *Proc. Ocean Drill. Program Sci. Results*, 113–125.

Alt J. C., Anderson T. F. and Bonnell L. (1989) The geochemistry of sulfur in a 1.3 km section of hydrothermally altered oceanic crust, DSDP Hole 504B. *Geochim. Cosmochim. Acta* **53**, 1011–1023.

Alt J. C., Davidson G. J., Teagle D. A. H. and Karson J. A. (2003) Isotopic composition of gypsum in the Macquarie Island ophiolite: Implications for the sulfur cycle and the subsurface biosphere in oceanic crust. *Geology* **31**, 549–552.

Alt J. C., Laverne C., Coggon R. M., Teagle D. A. H., Banerjee N. R., Morgan S., Smith-Duque C. E., Harris M. and Galli L. (2010) Subsurface structure of a submarine hydrothermal system in ocean crust formed at the East Pacific Rise, ODP/IODP Site 1256. *Geochem. Geophys., Geosyst.*, 11.

Alt J. C., Laverne C., Vanko D. A., Tartarotti P., Teagle D. A. H., Bach W., Zuleger E., Erzinger J., Honnorez J. and Pezard P. A. (1996) Hydrothermal alteration of a section of upper oceanic crust in the Eastern Equatorial Pacific: a synthesis of results from site 504 (DSDP Legs 69, 70, and 83, and ODP Legs 111, 137,140, and 148). *Proceedings of the Ocean Drilling Program, scientific results*, 417–434.

Alt J. C. and Shanks, III, W. C. (2003) Serpentinization of abyssal peridotites from the MARK area, Mid-Atlantic Ridge: sulfur geochemistry and reaction modeling. *Geochim. Cosmochim. Acta* **67**, 641–653.

Alt J. C., Shanks, III, W. C. and Jackson M. C. (1993) Cycling of sulfur in subduction zones: The geochemistry of sulfur in the Mariana Island Arc and back-arc trough. *Earth Planet. Sci. Lett.* **119**, 477–494.

Alt J. C. and Shanks W. C. (2011) Microbial sulfate reduction and the sulfur budget for a complete section of altered oceanic basalts, IODP Hole 1256D (eastern Pacific). *Earth Planet. Sci. Lett.* **310**, 73–83.

Armstrong J. T. (1991) Quantitative elemental analysis of individual microparticles with electron beam instruments. *Electron probe quantitation. Springer*, 261–315.

Audétat A., Pettke T. and Dolejš D. (2004) Magmatic anhydrite and calcite in the ore-forming quartz-monzodiorite magma at Santa Rita, New Mexico (USA): genetic constraints on porphyry-Cu mineralization. *Lithos* **72**, 147–161.

Balan E., Blanchard M., Pinilla C. and Lazzeri M. (2014) First-principles modeling of sulfate incorporation and 34S/32S isotopic fractionation in different calcium carbonates. *Chem. Geol.* **374**, 84–91.

Bali E., Aradi L. E., Zierenberg R. A., Diamond L. W., Pettke T., Szabó Á., Guðfinnsson G. H., Friðleifsson G. O. and Szabó C. (2020) Geothermal energy and ore-forming potential of 600 °C mid-ocean-ridge hydrothermal fluids. *Geology*.

Barker A. K., Coogan L. A. and Gillis K. M. (2010) Insights into the behaviour of sulphur in mid-ocean ridge axial hydrothermal systems from the composition of the sheeted dyke complex at Pito Deep. *Chem. Geol.* **275**, 105–115.

Barker A. K., Coogan L. A., Gillis K. M. and Weis D. (2008) Strontium isotope constraints on fluid flow in the sheeted dike complex of fast spreading crust: Pervasive fluid flow at Pito Deep. *Geochem., Geophys., Geosyst.*, 9.

Bernard A., Knittel U., Weber B., Weis D., Albrecht A., Hattori K., Klein J. and Oles D. (1996) Petrology and geochemistry of the 1991 eruption products of Mount Pinatubo. *Fire and mud: eruptions and lahars of Mount Pinatubo, Philippines*, 767–797.

Bernasconi S. M., Meier I., Wohlwend S., Brack P., Hochuli P. A., Bläsi H., Wortmann U. G. and Ramseyer K. (2017) An evaporite-based high-resolution sulfur isotope record of Late Permian and Triassic seawater sulfate. *Geochim. Cosmochim. Acta* **204**, 331–349.

Bickle M. J. and Teagle D. A. H. (1992) Strontium alteration in the Troodos ophiolite: implications for fluid fluxes and geochemical transport in mid-ocean ridge hydrothermal systems. *Earth Planet. Sci. Lett.* **113**, 219–237.

Botz R., Winckler G., Bayer R., Schmitt M., Schmidt M., Garbe-Schönberg D., Stoffers P. and Kristjansson J. K. (1999) Origin of trace gases in submarine hydrothermal vents of the Kolbeinsey Ridge, north Iceland. *Earth and Planet. Sci. Lett.* **171**, 83–93.

Bruland K. W. (1983) Trace elements in seawater. In *Chemical Oceanography* (eds. J. P. Riley and R. Chester). Academic Press Inc., (London) Ltd., London, pp. 157–220.

Budakoglu M. and Pratt L. M. (2005) Sulfur-isotope distribution and contamination related to the Balya Pb-Zn Mine in Turkey. *Environ. Geol.* **47**, 773–781.

Cabral R. A., Jackson M. G., Rose-Koga E. F., Koga K. T., Whitehouse M. J., Antonelli M. A., Farquhar J., Day J. M. D. and Hauri E. H. (2013) Anomalous sulphur isotopes in plume lavas reveal deep mantle storage of Archaean crust. *Nature* **496**, 490–493.

Chambefort I., Dilles J. H. and Kent A. R. (2008) Anhydrite-bearing andesite and dacite as a source for sulfur in magmatic-hydrothermal mineral deposits. *Geology* **36**, 719–722.

Chan L.-H., Alt J. C. and Teagle D. A. H. (2002) Lithium and lithium isotope profiles through the upper oceanic crust: a study of seawater-basalt exchange at ODP Sites 504B and 896A. *Earth Planet. Sci. Lett.* **201**, 187–201.

Chiba H., Kusakabe M., Hirano S.-I., Matsuo S. and Somiya S. (1981) Oxygen isotope fractionation factors between anhydrite and water from 100 to 550 °C. *Earth Planet. Sci. Lett.* **53**, 55–62.

Chiba H. and Sakai H. (1985) Oxygen isotope exchange rate between dissolved sulfate and water at hydrothermal temperatures. *Geochim. Cosmochim. Acta* **49**, 993–1000.

Chiba, H., Uchiyama, N. and Teagle, D.A.H. (1998) Stable isotope study of anhydrite and sulfide minerals at the TAG hydrothermal mound, Mid-Atlantic Ridge, 26°N, in: P.M. Herzig, S.E. Humphris, D.J. Miller, R.A. Zierenberg (Eds): Proceedings - Ocean Drilling Program Scientific Results 158, 85-90

Coogan L. A., Daëron M. and Gillis K. M. (2019) Seafloor weathering and the oxygen isotope ratio in seawater: insight from whole-rock $\delta^{18}O$ and carbonate $\delta^{18}O$ and $\Delta47$ from the Troodos ophiolite. *Earth Planet. Sci. Lett.* **508**, 41–50.

Coogan L. A. and Gillis K. M. (2018) Low-temperature alteration of the seafloor: impacts on ocean chemistry. *Ann. Rev. Earth Planet. Sci.* **46**, 21–45.

Craddock P. R. and Bach W. (2010) Insights to magmatic–hydrothermal processes in the Manus back-arc basin as recorded by anhydrite. *Geochim. Cosmochim. Acta* **74**, 5514–5536.

De Hoog J. C. M., Taylor B. E. and Van Bergen M. J. (2001) Sulfur isotope systematics of basaltic lavas from Indonesia: implications for the sulfur cycle in subduction zones. *Earth Planet. Sci. Lett.* **189**, 237–252.

Edwards K., Fisher A. and Wheat C. G. (2012) The deep subsurface biosphere in igneous ocean crust: frontier habitats for microbiological exploration. *Frontiers Microbiology* **3**, 8.

Elderfield H. and Schultz A. (1996) Mid-ocean ridge hydrothermal fluxes and the chemical composition of the ocean. *Ann. Rev. Earth Planet. Sci.* **24**, 191–224.

Eldridge D. L., Guo W. and Farquhar J. (2016) Theoretical estimates of equilibrium sulfur isotope effects in aqueous sulfur systems: highlighting the role of isomers in the sulfite and sulfoxylate systems. *Geochim. Cosmochim. Acta* **195**, 171–200.

Flóvenz Ó. G. and Gunnarsson K. (1991) Seismic crustal structure in Iceland and surrounding area. *Tectonophysics* **189**, 1–17.

Franzson H., Thordarson S., Björnsson G., Gudlaugsson S. T., Richter B., Fridleifsson G. O. and Thorhallsson S. (2002) Reykjanes high-temperature field, SW-Iceland: Geology and hydrothermal alteration of well RN-10. *Workshop on Geothermal Reservoir Engineering*, 233–240.

Friðleifsson G. Ó., Elders W. A., Zierenberg R. A., Fowler A. P. G., Weisenberger T. B., Mesfin K. G., Sigurðsson Ó., Níelsson S., Einarsson G. and Óskarsson F. (2020) The Iceland Deep Drilling Project at Reykjanes: Drilling into the root zone of a black smoker analog. *J. Volcanology Geotherm. Res.* **391** 106435.

German C. R., Briem J., Chin C., Danielsen M., Holland S., James R., Jónsdóttir A., Ludford E., Moser C. and Ólafsson J. M. R. P. (1994) Hydrothermal activity on the Reykjanes Ridge: the Steinahóll vent-field at 63°06′ N. *Earth Planet. Sci. Lett.* **121**, 647–654.

Gillis K. M., Muehlenbachs K., Stewart M., Gleeson T. and Karson J. (2001) Fluid flow patterns in fast spreading East Pacific Rise crust exposed at Hess Deep. *J. Geophys. Res.: Solid Earth* **106**, 26311–26329.

Grose C. J. and Afonso J. C. (2013) Comprehensive plate models for the thermal evolution of oceanic lithosphere. *Geochem., Geophys., Geosyst.* **14**, 3751–3778.

Gunnarsson-Robin, J., Stefánsson, A. and Kleine, B.I. (2018) IsoGem: an isotope geochemical modeling program, Goldschmidt Boston.

Gunnarsson-Robin J., Stefánsson A., Ono S. and Torssander P. (2017) Sulfur isotopes in Icelandic thermal fluids. *J. Volcanology Geotherm. Res.* **346**, 161–179.

Halldórsson S. A., Ranta E., Gunnarsson-Robin J., Bali E., Caracciolo A., Ono S., Jeon H., Whitehouse M. J., Hartley M. E., Dhaliwal J. K., Matthews S. and Stefánsson A. (2020) *Assessing sulfur isotope variability in the Icelandic mantle: evidence from subglacial glasses and melt inclusions*. Goldschmidt Virtual 2020, Honolulu, USA.

Hardardottir V., Hedenquist J., Hannington M., Brown K., Fridriksson T. and Thorhallsson S. (2010) Composition of reservoir liquid and metals in pipeline scale, Reykjanes geothermal system, SW Iceland. *Proc. World Geotherm. Congress*, 1–5.

Harris M., Coggon R. M., Wood M., Smith-Duque C. E., Henstock T. J. and Teagle D. A. H. (2017) Hydrothermal cooling of the ocean crust: Insights from ODP Hole 1256D. *Earth Planet. Sci. Lett.* **462**, 110–121.

Heft K. L., Gillis K. M., Pollock M. A., Karson J. A. and Klein E. M. (2008) Role of upwelling hydrothermal fluids in the development of alteration patterns at fast spreading ridges: Evidence from the sheeted dike complex at Pito Deep. *Geochem., Geophys., Geosyst.* **9**, 1–21.

Honnorez J. (1981) The aging of the oceanic crust at low temperature. In *Oceanic Lithosphere* (ed. C. Emiliani). Wiley, pp. 525–587.

Honnorez J., Laverne C., Hubberten H.-W., Emmermann R. and Muehlenbachs K. (1983) Alteration processes in layer 2 basalts from Deep Sea Drilling Project Hole 504B, Costa Rica Rift. *Initial Reports of Deep Sea Drilling Projects* **69**, 509–546.

Humphris S. E., Herzig P. M., Miller D. J., Alt J. C., Becker K., Brown D., Brugmann G., Chiba H., Fouquet Y., Gemmell J. B., Guerin G., Hannington M. D., Holm N. G., Honnorez J. J., Iturrino G. J., Knott R., Ludwig R., Nakamura K., Petersen S., Reysenbach A.-L., Rona P. A., Smith S., Sturz A. A., Tivey M. K. and Zhao X. (1995) The internal structure of an active seafloor massive sulphide deposit. *Nature* **377**, 713–716.

Ilyinskaya E., Mobbs S., Burton R., Burton M., Pardini F., Pfeffer M. A., Purvis R., Lee J., Bauguitte S. and Brooks B. (2018) Globally significant CO2 emissions from Katla, a subglacial volcano in Iceland. *Geophys. Res. Lett.* **45**, 1.

Imai A., Listanco E. L. and Fujii T. (1996) *Highly oxidized and sulfur-rich dacitic magma of Mount Pinatubo: implication for metallogenesis of porphyry copper mineralization in the western Luzon Arc*. Eruptions and lahars of Mount Pinatubo, Philippines, Fire and mud, pp. 865–874.

Ishihara S. and Sasaki A. (1989) Sulfur isotopic ratios of the magnetite-series and ilmenite-series granitoids of the Sierra Nevada batholith - a reconnaissance study. *Geology* **17**, 788–791.

Jackson M. D., Gudmundsson M. T., Weisenberger T. B., Rhodes J. M., Stefánsson A., Kleine B. I., Lippert P. C., Marquardt J. M., Reynolds H. I., Kück J., Marteinsson V. T., Vannier P., Bach W., Barich A., Bergsten P., Bryce J. G., Cappelletti P., Couper S., Fahnestock M. F., Gorny C. F., Grimaldi C., Groh M., Guðmundsson Á., Gunnlaugsson Á. T., Hamlin C., Högnadóttir T., Jónasson K., Jónsson S. S., Jørgensen S. L., Klonowski A. M., Marshall B., Massey E., McPhie J., Moore J. G., Ólafsson E. S., Onstad S. L., Perez V., Prause S., Snorrason S. P., Türke A., White J. D. L. and Zimanowski B. (2019) SUSTAIN drilling at Surtsey volcano, Iceland, tracks hydrothermal and microbiological interactions in basalt 50 years after eruption. *Scientific Drilling* **25**, 35–46.

Jakobsson S. P., Leonardsen E. S., Zunic T. B. and Jonsson S. S. (2008) *Encrustations from three recent volcanic eruptions in Iceland: The 1963–1967 Surtsey, the 1973 Eldfell and the 1991 Hekla eruptions*. Náttúrufræðistofnun Íslands, Reykjavík.

Jakobsson S. P. and Moore J. G. (1986) Hydrothermal minerals and alteration rates at Surtsey volcano, Iceland. *Geol. Soc. Am. Bull.* **97**, 648–659.

Kadko D., Baross J. and Alt J. (1995) The magnitude and global implications of hydrothermal flux. In *Seafloor Hydrothermal Systems: Physical, Chemical, Biological, and Geological Interactions* (eds. S. E. Humphris, R. A. Zierenberg, L. S. Mullineaux and R. E. Thomson). Geophysical Monograph Series, pp. 446–466.

Kawada Y. and Yoshida S. (2010) Formation of a hydrothermal reservoir due to anhydrite precipitation in an arc volcano hydrothermal system. *J. Geophys. Res.: Solid Earth* **115**, B11106.

Kelemen P. B., Matter J. M., Teagle D. A. H., Coggon J. A. and the Oman Drilling Project Science Team (2020a) Site GT1: layered cumulate gabbros and deep fault zones. In *Proceedings of the Oman Drilling Project* (eds. P. B. Kelemen, J. M. Matter, D. A. H. Teagle and J. A. Coggon). International Ocean Discovery Program, College Station, TX.

Kelemen, P.B., Matter, J.M., Teagle, D.A.H., Coggon, J.A. and the Oman Drilling Project Science Team (2020b) Site GT2: foliated to layered gabbro transition. In: Kelemen, P.B., Matter, J.M., Teagle, D.A.H., Coggon, J.A., al., e. (Eds.), Proceedings of the Oman Drilling Project. International Ocean Discovery Program, College Station, TX.

Kleine B. I., Stefánsson A., Halldórsson S. A. and Barnes J. D. (2020a) Impact of fluid-rock interaction on water uptake of the Icelandic crust: Implications for the hydration of the oceanic crust and the subducted water flux. *Earth Planet. Sci. Lett.* **538** 116210.

Kleine B. I., Stefánsson A., Kjartansdóttir R., Prause S., Weisenberger T. B., Reynolds H. I., Sveinbjörnsdóttir Á. E., Jackson M. D. and Gudmundsson M. T. (2020b) The Surtsey volcano geothermal system: An analogue for seawater-oceanic crust interaction with implications for the elemental budget of the oceanic crust. *Chem. Geol.* **550** 119702.

Kusakabe M., Chiba H. and Ohmoto H. (1982) Stable isotopes and fluid inclusion study of anhydrite from the East Pacific Rise at 21°N. *Geochem. J.* **16**, 89–95.

Kusakabe, M., Shibata, T., Yamamoto, M., Mayeda, S., Kagami, H., Honma, H., Masuda, H. and Sakai, H. (1989) Petrology and isotope characteristics (H, O, S, Sr, and Nd) of basalts from Ocean Drilling Program Hole 504B, Leg 111, Costa Rica Rift, Becker, K., Sakai, H., et al., Proc. ODP, Sci. Results. Citeseer, pp. 47–60.

Lefticariu L., Pratt L. M. and Ripley E. M. (2006) Mineralogic and sulfur isotopic effects accompanying oxidation of pyrite in millimolar solutions of hydrogen peroxide at temperatures from 4 to 150 °C. *Geochim. Cosmochim. Acta* **70**, 4889–4905.

Lever M. A., Rouxel O., Alt J. C., Shimizu N., Ono S., Coggon R. M., Shanks W. C., Lapham L., Elvert M. and Prieto-Mollar X. (2013) Evidence for microbial carbon and sulfur cycling in deeply buried ridge flank basalt. *Science* **339**, 1305–1308.

Li J.-L., Schwarzenbach E. M., John T., Ague J. J., Huang F., Gao J., Klemd R., Whitehouse M. J. and Wang X.-S. (2020) Uncovering and quantifying the subduction zone sulfur cycle from the slab perspective. *Nat. Commun.* **11**, 1–12.

Lilley M. D., Butterfield D. A., Lupton J. E. and Olson E. J. (2003) Magmatic events can produce rapid changes in hydrothermal vent chemistry. *Nature* **422**, 878.

Lowell R. P., Yao Y. and Germanovich L. N. (2003) Anhydrite precipitation and the relationship between focused and diffuse flow in seafloor hydrothermal systems. *J. Geophys. Res.: Solid Earth* **108**.

Luhr J. F. (2008) Primary igneous anhydrite: Progress since its recognition in the 1982 El Chichón trachyandesite. *J. Volcanology Geotherm. Res.* **175**, 394–407.

Luhr J. F. and Logan M. A. V. (2002) Sulfur isotope systematics of the 1982 El Chichón trachyandesite: An ion microprobe study. *Geochim. Cosmochim. Acta* **66**, 3303–3316.

Marks N., Schiffman P. and Zierenberg R. A. (2011) High-grade contact metamorphism in the Reykjanes geothermal system: Implications for fluid-rock interactions at mid-oceanic ridge spreading centers. *Geochem., Geophys., Geosyst.* **12**, 1–25.

Marks N., Schiffman P., Zierenberg R. A., Franzson H. and Fridleifsson G. Ó. (2010) Hydrothermal alteration in the Reykjanes geothermal system: Insights from Iceland deep drilling program well RN-17. *J. Volcanology Geotherm. Res.* **189**, 172–190.

Martin A. J., McDonald I., Jenkin G. R. T., McFall K. A., Boyce A. J., Jamieson J. W. and MacLeod C. J. (2021) A missing link between ancient and active mafic-hosted seafloor hydrothermal systems – Magmatic volatile influx in the exceptionally preserved Mala VMS deposit, Troodos, Cyprus. *Chem. Geol.* **567** 120127.

McDermott J. M., Ono S., Tivey M. K., Seewald J. S., Shanks, III, W. C. and Solow A. R. (2015) Identification of sulfur sources and isotopic equilibria in submarine hot-springs using multiple sulfur isotopes. *Geochim. Cosmochim. Acta* **160**, 169–187.

McDuff R. E. and Edmond J. M. (1982) On the fate of sulfate during hydrothermal circulation at mid-ocean ridges. *Earth Planet. Sci. Lett.* **57**, 117–132.

Mottl, M. J. (1989) Hydrothermal convection, reaction, and diffusion in sediments on the Costa Rica Rift flank: pore-water evidence from ODP Sites 677 and 678, Becker, K., Sakai, H., et al., Proc. ODP, Sci. Results, pp. 195-213.

Mottl M. J. (2003) Partitioning of energy and mass fluxes between mid-ocean ridge axes and flanks at high and low temperature. *Energy and Mass Transfer in Marine Hydrothermal Systems*, 271–286.

Mottl M. J. and Wheat C. G. (1994) Hydrothermal circulation through mid-ocean ridge flanks: Fluxes of heat and magnesium. *Geochim. Cosmochim. Acta* **58**, 2225–2237.

Mottl M. J., Wheat G., Baker E., Becker N., Davis E., Feely R., Grehan A., Kadko D., Lilley M. and Massoth G. (1998) Warm springs discovered on 3.5 Ma oceanic crust, eastern flank of the Juan de Fuca Ridge. *Geology* **26**, 51–54.

Muehlenbachs K. and Clayton R. N. (1976) Oxygen isotope composition of the oceanic crust and its bearing on seawater. *J. Geophys. Res.* **81**, 4365–4369.

Nehlig P. and Juteau T. (1988) Flow porosities, permeabilities and preliminary data on fluid inclusions and fossil thermal gradients in the crustal sequence of the Sumail ophiolite (Oman). *Tectonophysics* **151**, 199–221.

Nielsen S. G., Rehkämper M., Teagle D. A. H., Butterfield D. A., Alt J. C. and Halliday A. N. (2006) Hydrothermal fluid fluxes calculated from the isotopic mass balance of thallium in the ocean crust. *Earth Planet. Sci. Lett.* **251**, 120–133.

Ohmoto H. and Goldhaber M. B. (1997) Sulfur and carbon isotopes. In *Geochemistry of Hydrothermal Ore Deposits* (ed. H. L. Barnes). Wiley, New York, pp. 517–612.

Ohmoto H. and Lasaga A. C. (1982) Kinetics of reactions between aqueous sulfates and sulfides in hydrothermal systems. *Geochim. Cosmochim. Acta* **46**, 1727–1745.

Ólafsson J., Thors K. and Cann J. (1991) A sudden cruise off Iceland. *Ridge Events* **2**, 35–38.

Ono S., Shanks, III, W. C., Rouxel O. J. and Rumble D. (2007) S-33 constraints on the seawater sulfate contribution in modern seafloor hydrothermal vent sulfides. *Geochim. Cosmochim. Acta* **71**, 1170–1182.

Óskarsson N. (1981) The chemistry of Icelandic lava incrustations and the latest stages of degassing. *J. Volcanology Geotherm. Res.* **10**, 93–111.

Padilla, E.K., Stefánsson, A. and Fridriksson, T. (2012) Sulphur precipitation in the Reykjanes geothermal system, Iceland, Proceedings of Thirty-Seventh Workshop on Geothermal Reservoir Engineering Stanford University

Palmer M. R. and Edmond J. M. (1989) The strontium isotope budget of the modern ocean. *Earth Planet. Sci. Lett.* **92**, 11–26.

Palmer M. R., Ludford E. M., German C. R. and Lilley M. D. (1995) Dissolved methane and hydrogen in the Steinaholl hydrothermal plume, 63°N, Reykjanes Ridge. *Geological Society, London, Special Publications* **87**, 111–120.

Parkhurst D. L. and Appelo C. (1999) User's guide to PHREEQC (Version 2): A computer program for speciation, batch-reaction, one-dimensional transport, and inverse geochemical calculations. *Water-resources Investigations Report* **99**, 312.

Paytan A., Kastner M., Campbell D. and Thiemens M. H. (2004) Seawater sulfur isotope fluctuations in the Cretaceous. *Science* **304**, 1663–1665.

Peters M., Strauss H., Farquhar J., Ockert C., Eickmann B. and Jost C. L. (2010) Sulfur cycling at the Mid-Atlantic Ridge: A multiple sulfur isotope approach. *Chem. Geol.* **269**, 180–196.

Pope E. C., Bird D. K., Arnórsson S., Fridriksson T., Elders W. A. and Fridleifsson G. Ó. (2009) Isotopic constraints on ice age fluids in active geothermal systems: Reykjanes, Iceland. *Geochim. Cosmochim. Acta* **73**, 4468–4488.

Prause S., Weisenberger T. B., Cappelletti P., Grimaldi C., Rispoli C., Jónasson K., Jackson M. D. and Gudmundsson M. T. (2020) Alteration progress within the Surtsey hydrothermal system, SW Iceland–A time-lapse petrographic study of cores drilled in 1979 and 2017. *J. Volcanol. Geotherm. Res.* **392** 106754.

Reuschel M., Melezhik V. A., Whitehouse M. J., Lepland A., Fallick A. E. and Strauss H. (2012) Isotopic evidence for a sizeable seawater sulfate reservoir at 2.1 Ga. *Precambrian Res.* **192**, 78–88.

Rye R. O., Luhr J. F. and Wasserman M. D. (1984) Sulfur and oxygen isotopic systematics of the 1982 eruptions of El Chichón Volcano, Chiapas, Mexico. *J. Volcanology Geotherm. Res.* **23**, 109–123.

Saal A. E., Hauri E. H., Langmuir C. H. and Perfit M. R. (2002) Vapour undersaturation in primitive mid-ocean-ridge basalt and the volatile content of Earth's upper mantle. *Nature* **419**, 451–455.

Sasaki A. and Ishihara S. (1979) Sulfur isotopic composition of the magnetite-series and ilmenite-series granitoids in Japan. *Contrib. Mineral. Petrol.* **68**, 107–115.

Seal R. R. (2006) Sulfur isotope geochemistry of sulfide minerals. *Rev. Mineral. Geochem.* **61**, 633–677.

Seal R. R., Alpers C. N. and Rye R. O. (2000a) Stable isotope systematics of sulfate minerals. *Rev. Mineral. Geochem.* **40**, 541–602.

Seal R. R., Hammarstrom J. M. and Foley N. K. (2000b) Geoenvironmental models for seafloor base-and precious-metal massive sulfide deposits. In *5th International Conference on Acid Rock Drainage*, pp. 151–160.

Seyfried, Jr, W. and Bischoff J. (1979) Low temperature basalt alteration by sea water: an experimental study at 70 C and 150 C. *Geochim. Cosmochim. Acta* **43**, 1937–1947.

Shanks, III, W. C. (2001) Stable isotopes in seafloor hydrothermal systems: vent fluids, hydrothermal deposits, hydrothermal alteration, and microbial processes. *Rev. Mineral. Geochem.* **43**, 469–525.

Shanks, III, W. C., Bischoff J. L. and Rosenbauer R. J. (1981) Seawater sulfate reduction and sulfur isotope fractionation in basaltic systems: interaction of seawater with fayalite and magnetite at 200–350 C. *Geochim. Cosmochim. Acta* **45**, 1977–1995.

Shipp W. G. and Zierenberg R. A. (2008) Pathways of acid mine drainage to Clear Lake: implications for mercury cycling. *Ecol. Appl.* **18**, A29–A54.

Sigvaldason G. E. and Elísson G. (1968) Collection and analysis of volcanic gases at Surtsey Iceland. *Geochim. Cosmochim. Acta* **32**, 797–805.

Skikazono N., Holland H. D. and Quirk R. F. (1983) *Anhydrite in Kuroko deposits: Mode of occurrence and depositional mechanisms*. Economic Geology Monograph, New Haven.

Sleep N. H. (1991) Hydrothermal circulation, anhydrite precipitation, and thermal structure at ridge axes. *J. Geophys. Res.: Solid Earth* **96**, 2375–2387.

Spencer R. J. (2000) Sulfate minerals in evaporite deposits. *Rev. Mineral. Geochem.* **40**, 173–192.

Staudigel H. (2014) Chemical fluxes from hydrothermal alteration of the oceanic crust. In *The Crust* (ed. R. R. L). Elsevier, Oxford, pp. 583–606.

Stefánsson A., Hilton D. R., Sveinbjörnsdóttir Á. E., Torssander P., Heinemeier J., Barnes J. D., Ono S., Halldórsson S. A., Fiebig J. and Arnórsson S. (2017a) Isotope systematics of Icelandic thermal fluids. *J. Volcanology Geotherm. Res.* **337**, 146–164.

Stefánsson A., Keller N. S., Gunnarsson-Robin J. and Ono S. (2015) Multiple sulfur isotope systematics of Icelandic geothermal fluids and the source and reactions of sulfur in volcanic geothermal systems at divergent plate boundaries. *Geochim. Cosmochim. Acta* **165**, 307–323.

Stefánsson A., Stefánsdóttir G., Keller N. S., Barsotti S., Sigurdsson Á., Thorláksdóttir S. B., Pfeffer M. A., Eiríksdóttir E. S., Jónasdóttir E. B. and von Löwis S. (2017b) Major impact of volcanic gases on the chemical composition of precipitation in Iceland during the 2014–2015 Holuhraun eruption. *J. Geophys. Res.: Atmos.* **122**, 1971–1982.

Stein C. A. and Stein S. (1994) Constraints on hydrothermal heat flux through the oceanic lithosphere from global heat flow. *J. Geophys. Res.: Solid Earth* **99**, 3081–3095.

Stern C. R., Funk J. A., Skewes M. A. and Arévalo A. (2007) Magmatic anhydrite in plutonic rocks at the El Teniente Cu-Mo deposit, Chile, and the role of sulfur-and copper-rich magmas in its formation. *Econ. Geology* **102**, 1335–1344.

Strauss H., Melezhik V. A., Reuschel M., Fallick A. E., Lepland A. and Rychanchik D. V. (2013) 7.5 Abundant Marine Calcium Sulphates: Radical Change of Seawater Sulphate Reservoir and Sulphur Cycle, Reading the Archive of Earth's Oxygenation. *Springer*, 1169–1194.

Sturkell E., Brandsdottir B., Shimamura H. and Mochizuki M. (1992) Seismic crustal structure along the Axarfjörður trough at the eastern margin of the Tjörnes fracture zone. *N-Iceland. Jökull*, 13–24.

Taylor B. E. and Wheeler M. C. (1994) Sulfur-and oxygen-isotope geochemistry of acid mine drainage in the western United States: field and experimental studies revisited. In *Environmental Geochemistry of Sulfide Oxidation* (eds. C. N. Alpers and D. W. Blowes). ACS Publications, pp. 481–514.

Teagle, D. A. H., Alt, J. C., Bach, W., Halliday, A. and Erzinger J. (1996) Alteration of the upper ocean crust in a ridge flank hydrothermal up-flow zone: Mineral, chemical, and isotopic constraints from ODP Hole 896A. In: J. C. Alt, H. Kinoshita, L. B. Stokking, P. J. Michael (Eds.): Proceedings of the Ocean Drilling Program, Scientific Results 148, 119-150.

Teagle D. A. H., Alt J. C., Chiba H., Humphris S. E. and Halliday A. N. (1998a) Strontium and oxygen isotopic constraints on fluid mixing, alteration and mineralization in the TAG hydrothermal deposit. *Chem. Geol.* **149**, 1–24.

Teagle D. A. H., Alt J. C. and Halliday A. N. (1998b) Tracing the chemical evolution of fluids during hydrothermal recharge: Constraints from anhydrite recovered in ODP Hole 504B. *Earth Planet. Sci. Lett.* **155**, 167–182.

Teagle D. A. H., Alt J. C. and Halliday A. N. (1998c) Tracing the evolution of hydrothermal fluids in the upper oceanic crust: Sr-isotopic constraints from DSDP/ODP Holes 504B and 896A. *Geol. Soc., London, Special Publications* **148**, 81–97.

Teagle, D. A. H., Alt, J. C., Umino, S., Miyashita, S., Banerjee, N. R., Wilson, D. S. and the Expedition 309/312 Scientists (2006) Superfast Spreading Rate Crust 2 and 3 Proc. Integrated Ocean Drill. Program, 309/312.

Teagle D. A. H., Bickle M. J. and Alt J. C. (2003) Recharge flux to ocean-ridge black smoker systems: a geochemical estimate from ODP Hole 504B. *Earth Planet. Sci. Lett.* **210**, 81–89.

Thorarinsson S., Einarsson T., Sigvaldason G. and Elisson G. (1964) The submarine eruption off the Vestmann Islands 1963–64. *Bull. Volcanologique* **27**, 435–445.

Thordarson T. and Larsen G. (2007) Volcanism in Iceland in historical time: Volcano types, eruption styles and eruptive history. *J. Geodyn.* **43**, 118–152.

Torssander P. (1988) Sulfur isotope ratios of Icelandic lava incrustations and volcanic gases. *J. Volcanology Geotherm. Res.* **35**, 227–235.

Torssander P. (1989) Sulfur isotope ratios of Icelandic rocks. *Contrib. Mineral. Petrol.* **102**, 18–23.

Tostevin R., Turchyn A. V., Farquhar J., Johnston D. T., Eldridge D. L., Bishop J. K. B. and McIlvin M. (2014) Multiple sulfur isotope constraints on the modern sulfur cycle. *Earth Planet. Sci. Lett.* **396**, 14–21.

Ueda A. and Sakai H. (1984) Sulfur isotope study of Quaternary volcanic rocks from the Japanese Islands Arc. *Geochim. Cosmochim. Acta* **48**, 1837–1848.

Von Damm K., Edmond J., Grant B., Measures C., Walden B. and Weiss R. (1985) Chemistry of submarine hydrothermal solutions at 21° N, East Pacific Rise. *Geochim. Cosmochim. Acta* **49**, 2197–2220.

Von Damm K. L. (1990) Seafloor hydrothermal activity: black smoker chemistry and chimneys. *Ann. Rev. Earth Planet. Sci.* **18**, 173–204.

Von Damm K. L. (1995) Controls on the chemistry and temporal variability of seafloor hydrothermal fluids. *Seafloor Hydrothermal Systems: Physical, Chemical, Biological, and Geological Interactions* **91**, 222–247.

Von Damm K. L. (2000) Chemistry of hydrothermal vent fluids from 9–10 N, East Pacific Rise: "Time zero", the immediate posteruptive period. *J. Geophys. Res.: Solid Earth* **105**, 11203–11222.

Von Damm K. L., Edmond J. M. l., Grant B., Measures C. I., Walden B. and Weiss R. F. (1985) Chemistry of submarine hydrothermal solutions at 21°N, East Pacific Rise. *Geochim. Cosmochim. Acta* **49**, 2197–2220.

Von Damm K. L., Oosting S. E., Kozlowski R., Buttermore L. G., Colodner D. C., Edmonds H. N., Edmond J. M. and Grebmeier J. M. (1995) Evolution of East Pacific Rise hydrothermal vent fluids following a volcanic eruption. *Nature* **375**, 47.

Warren J. (1999) *Evaporites; Their Evolution and Economics*. Blackwells, Oxford.

Wheat C. G., Feely R. A. and Mottl M. J. (1996) Phosphate removal by oceanic hydrothermal processes: An update of the phosphorus budget in the oceans. *Geochim. Cosmochim. Acta* **60**, 3593–3608.

Wheat C. G. and Fisher A. T. (2008) Massive, low-temperature hydrothermal flow from a basaltic outcrop on 23 Ma seafloor of the Cocos Plate: Chemical constraints and implications. *Geochem. Geophys., Geosyst.*, 9.

Wheat C. G., Hartwell A. M., McManus J., Fisher A. T., Orcutt B. N., Schlicht L. E. M., Niedenzu S. and Bach W. (2019) Geology and fluid discharge at Dorado Outcrop, a low temperature ridge-flank hydrothermal system. *Geochem., Geophys., Geosyst.* **20**, 487–504.

Wheat C. G. and Mottl M. J. (2000) Composition of pore and spring waters from Baby Bare: Global implications of geochemical fluxes from a ridge flank hydrothermal system. *Geochim. Cosmochim. Acta* **64**, 629–642.

Wheat C. G. and Mottl M. J. (2004) Chapter 19: Geochemical fluxes through ridge flanks. In *Hydrolgeology of the Oceanic Lithosphere* (eds. E. Davis and H. Elderfield). Cambridge University Press, New York, pp. 627–658.

Woodhead J. D., Harmon R. S. and Fraser D. G. (1987) O, S, Sr, and Pb isotope variations in volcanic rocks from the Northern Mariana Islands: implications for crustal recycling in intra-oceanic arcs. *Earth Planet. Sci. Lett.* **83**, 39–52.

Zeebe R. E. (2010) A new value for the stable oxygen isotope fractionation between dissolved sulfate ion and water. *Geochim. Cosmochim. Acta* **74**, 818–828.

Zierenberg R. A., Fowler A. P. G., Friðleifsson G. Ó., Elders W. A. and Weisenberger T. B. (2017) Preliminary description of rocks and alteration in IDDP-2 drill core samples recovered from the Reykjanes Geothermal System, Iceland. *GRC Trans.* **41**, 1599–1615.

Associate editor: Damon A.H. Teagle